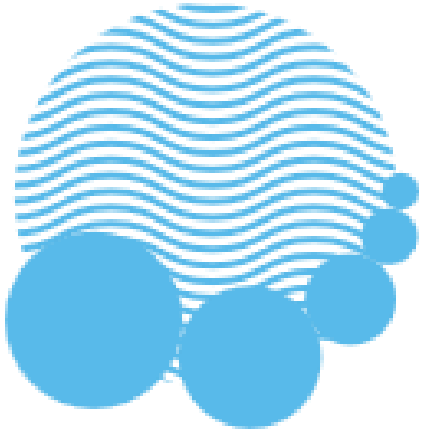

OFFSHORE ENERGY HUBS

CONTROL SOLUTIONS FOR STABLE HUB OPERATION

ABBREVIATIONS

AC: alternative current

DC: direct current

HVDC: high voltage direct current

MTDC: multi-terminal direct current

MMC: modular multilevel converter

SM: sub-module

EMT: electromagnetic transient

RMS: root mean square

PSCAD: power systems computer-aided design

GFM: grid-forming

GFL: grid-following

PI: proportional-integral

OEH: offshore energy hub

OWF: offshore wind farm

WPP: wind power plant

WP: work package

TABLE OF CONTENTS

1. Executive Summary 4
2. Introduction 4
3. Modelling and Control Design for AC and DC Hubs 4
3.1. Control Design for the AC Hub 5
3.1.1. Single-Loop Grid-Forming Control Scheme 7
3.1.2. Multiple-Loop Grid-Forming Control Scheme 8
3.2. Control Design for the DC Hub 9
3.2.1. Typical DC Voltage Control Scheme 10
3.2.2. DC-Droop Control Scheme 11
4. PSCAD Modelling and Simulations 13
4.1. AC Hub Model Development 13
4.1.1. Single-Loop Grid-Forming Control Scheme 15
4.1.2. Multiple-Loop Grid-Forming Control Scheme 15
4.2. Simulations of AC Hub in Different Cases 16
4.2.1. Single-Loop Grid-Forming Control Scheme 16
4.2.2. Multiple-Loop Grid-Forming Control Scheme 23
4.3. DC Hub Model Development 27
4.4. Simulations of DC Hub in Different Cases 28
4.5. Hybrid Hub Model Development 40
5. Power Factory Model 42
6. Model Comparison 44
7. Conclusions 47
8. References 48

1. EXECUTIVE SUMMARY

This report evaluates the offshore energy hub (OEH) with grid-forming (GFM) functionalities under many different operation modes in normal and abnormal scenarios, where the stable and robust control solutions of the OEH are the main research focus. Specifically, the electromagnetic transient (EMT) and the root mean square (RMS) simulation models are developed in PSCAD and Power Factory-DIgSILENT simulation software to evaluate the small-signal and transient stability of the OEH system.

2. INTRODUCTION

The decision to build the world's first two offshore energy islands (or hubs) is a cornerstone in reaching Denmark's climate targets and the beginning of a new era for green Danish technology export. The purpose of the Offshore Energy Hubs (OEH) project is to develop technical solutions that addressing several challenges related to offshore energy islands [1]. One of the key tasks in Work Package 2 (WP2) is to develop tools and control solutions for stable and resilient hub operation.

In the previous stage of this project (i.e., WP2, Task 2.1), three main OEH topologies were investigated, which are the alternating current (AC) hub, the direct current (DC) hub, and the hybrid hub [2]. The AC hub solution relies on an interconnected HVAC system to connect multiple point-to-point HVDC systems. The DC solution splits the HVDC system into offshore converters that supply smaller, islanded AC systems where the offshore WPPs are integrated, and interconnected DC systems that link converter poles of the same polarity. The hybrid solution combines both solutions by providing an interconnected AC system as well as a multi-terminal DC (MTDC) system, which enables the option to operate the hub in either AC- or DC-coupled mode. Previous studies have found that each of the three hub topologies has its advantages and disadvantages. So, each topology needs to be investigated further. Following the research outputs in Task 2.1, the AC hub topology is selected as the first priority to study in Task 2.2. Subsequently, the DC hub topology is selected as the second priority to study.

In the current stage of this project (i.e., Task 2.2), the main task is to develop simulation models of an OEH by using stable and robust control solutions. To achieve this project goal, PSCAD and Power Factory-DIgSILENT simulation tools are used to develop the OEH models. Besides, several mainstream grid-forming (GFM) control schemes are selected to study and compare their performance under normal and abnormal conditions. In the rest part of this report, detailed GFM control design, DC droop control design, and OEH models are introduced in Section 3. Simulation results of the developed PSCAD models will be presented in Section 4. The simulation results of the developed Power Factory models will be presented in Section 5. Two models are compared in Section 6. Finally, the report is concluded in Section 7.

3. MODELLING AND CONTROL DESIGN FOR AC AND DC HUBS

Following the research outputs in Task 2.1, this section will focus on offshore AC and DC hubs with an internal interconnector and two 2 GW HVDC systems.

3.1. CONTROL DESIGN FOR THE AC HUB

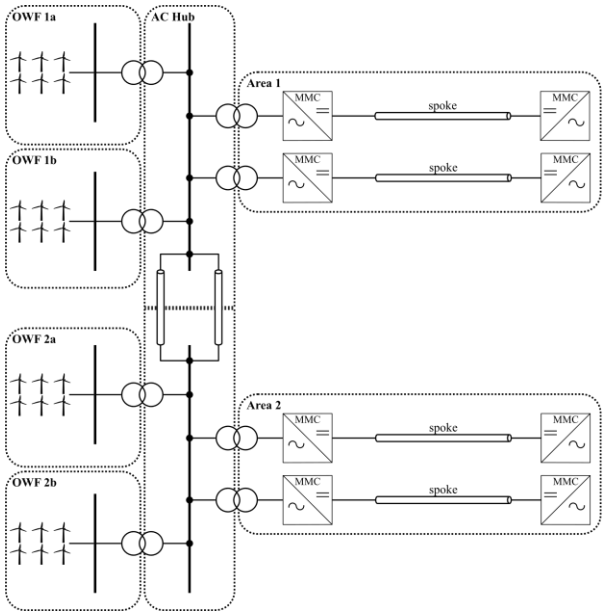

Figure 3.1: A general system configuration of the selected AC hub study case.

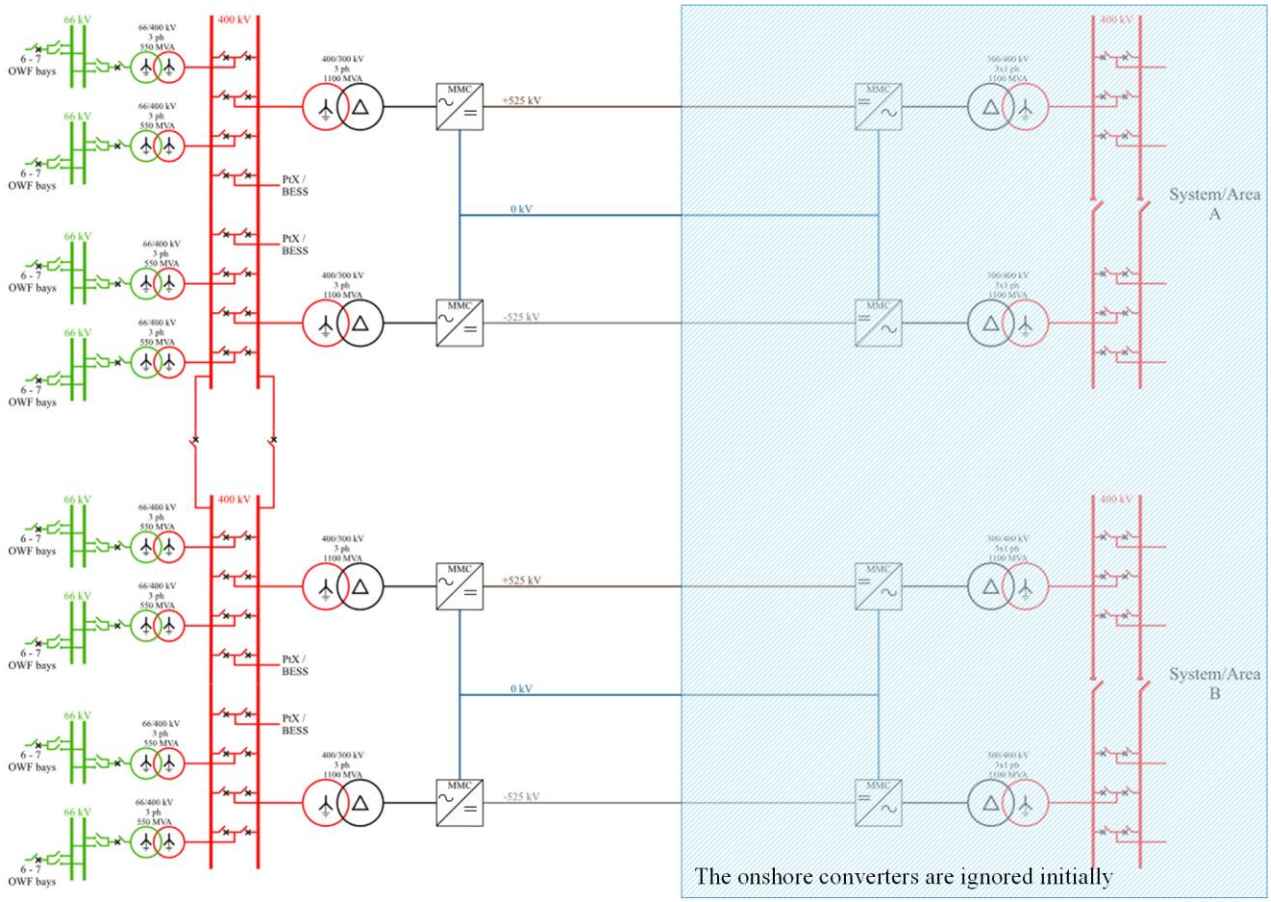

Figure 3.2: Detailed system configuration of the AC hub.

Figure 3.1 shows a general system configuration of the selected AC hub study case. The rated voltage of the offshore AC grid is 400 kV. The rated active power of the two bipolar HVDC transmission systems is 2 GW. Besides, the rated DC voltage of both HVDC systems is ±525 kV. Moreover, offshore wind farms are connected to the AC hub to inject power. In Figure 3.1, there are four offshore wind farms, and the rated power of each wind farm is 1 GW.

To be more specific, a more detailed system configuration of the selected AC hub study case is presented in Figure 3.2, where the rated power of each wind farm is 500 MW. The offshore wind farms are connected to 66 kV busbars, and three-phase Y-Y transformers are used to connect the offshore wind farms and the AC hub. The voltage ratio of the transformer is 66 kV/400 kV. Besides, the HVDC systems are connected to the AC hub through three-phase Y-Δ transformers, where the voltage ratio is 400 kV/300 kV. Since the offshore HVDC converters are in charge of establishing the offshore AC grid, the modelling and controller design of the offshore HVDC converters will be discussed in Section 3.1.

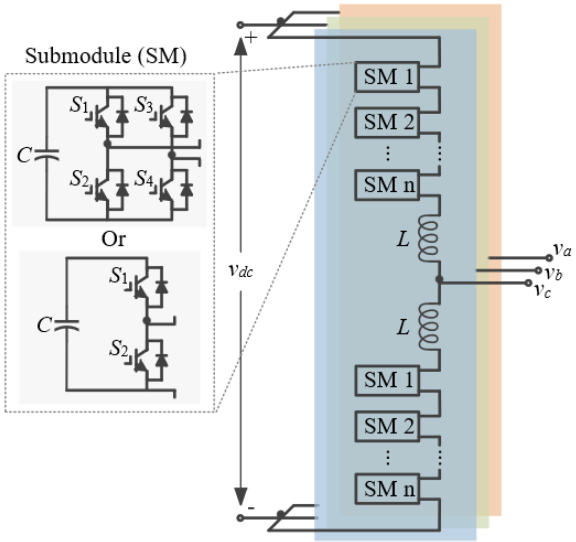

Figure 3.3: A typical configuration of the modular multilevel converter.

The scope of the AC hub study in this section is the modelling and control design of the offshore HVDC converter under normal conditions, while the scope of the DC hub study in the following section is the control design of the onshore HVDC converter. Besides, the additional control design for different fault scenarios will be investigated in the future. As shown in Figure 3.3, the topology of a single HVDC converter is a modular multilevel converter (MMC). It has three legs, and each leg has plenty of submodules (SM). For simplicity, a half-bridge converter is typically used in the SM [3]. Considering the main research interest in this project is to evaluate the high-level control interactions among different HVDC converters, the internal switching dynamics of the MMC are possible to be ignored.

As shown in Figure 3.4, MMC models are possibly being simplified at different levels [4]. Figure 3.4(a) shows a detailed switching model, while Figure 3.4(b)-(d) shows an equivalent circuit-based model, an average arm model, and an average leg model, respectively. For simplicity, the average leg model is selected initially to represent the MMC, while the detailed switching model will be considered in a later stage of this project. It is worth mentioning that the average leg model is selected to study the quasi-steady state scenarios with the time scale from seconds to tens of seconds. When studying the fault cases with the time scale of milliseconds, the detail switching model might be necessary.

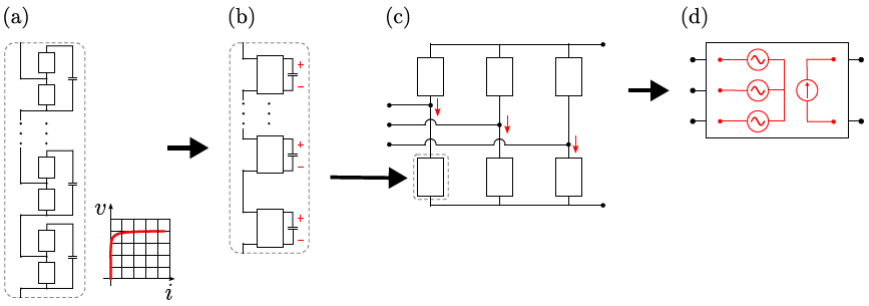

Figure 3.4: Simplified MMC models at different levels (a) Detailed switching model; (b) Equivalent circuit-based model; (c) Average arm model; (d) Average leg model.

After introducing the topologies of the offshore AC hub, the control strategies of the AC hub are worth being discussed emphatically. In fact, there are different ways to control the offshore wind farm, the offshore HVDC converter, and the onshore HVDC converter. For example, the first solution is that the offshore wind farm is a grid-following (GFL) unit, the offshore HVDC converter is a grid-forming (GFM) unit, and the onshore HVDC converter is used to control the DC-link voltage. Besides, the second solution is that the offshore wind farm is a GFM unit, the offshore HVDC converter is used to control the DC-link voltage, and the onshore HVDC converter is a GFM unit. Of course, there are other options. However, due to the time limitation in this project, the first solution is considered a baseline solution, and it will be selected as the current research focus. Therefore, in this case, the offshore wind farm is a GFL unit and the offshore HVDC converter is a GFM unit.

Regarding the GFM control strategy, so far many different GFM control strategies have been published in the existing literature, such as droop control [5], synchronverter [6], virtual synchronous generator [7], power synchronization control [8], synchronous power control [9], and virtual oscillator control [10]. Among these schemes, the droop-based control scheme attracts more attention, where a virtual impedance is usually used to improve the small-signal stability under normal conditions [11]. In this section, the droop-based single-loop GFM control scheme and multiple-loop GFM control scheme with virtual impedance are selected for controlling the offshore HVDC converter, respectively. The detailed GFM control schemes of these two selected GFM control methods will be introduced as follows.

3.1.1. Single-Loop Grid-Forming Control Scheme

The single-loop GFM control scheme with virtual impedance is presented in Figure 3.5. It mainly includes active and reactive power droop controllers. The P-ω droop control is used to control the active power. Then, the synchronization angle is generated by the angular frequency ω going through an integrator. Besides, the Q-V droop control is used to control the reactive power. A cascaded PI controller is also used to control the voltage magnitude and generate a voltage reference. To increase the robustness of the GFM control scheme, a virtual impedance is also added from the current feedback to the voltage reference. This simple control structure enables the basic GFM function during normal operation.

Regarding the control parameters of the single-loop GFM control scheme in Figure 3.5, it is flexible to choose different values for the control parameters. Based on previous research experience, the P-ω

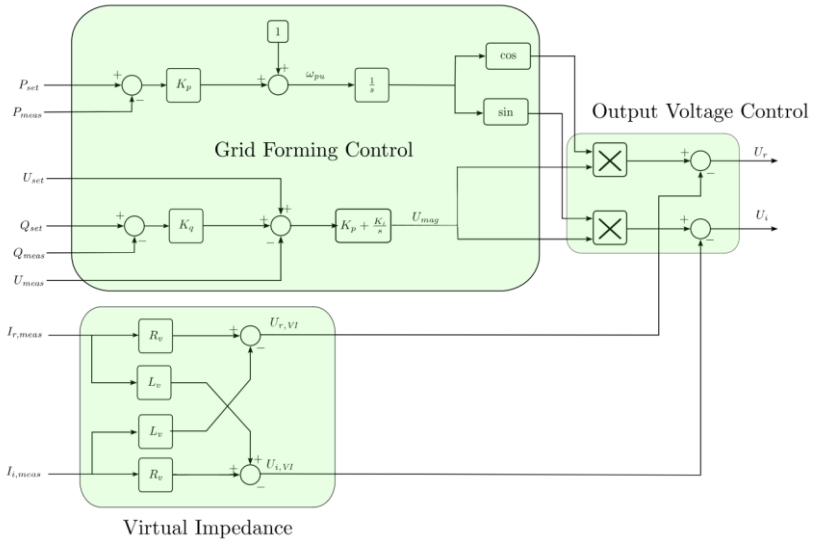

Figure 3.5: Single-loop grid-forming control scheme with virtual impedance.

droop coefficient can be designed within 1% ~ 5% of ω_N/P_N. And the Q-V droop coefficient can be designed within 1% ~ 10% of V_N/P_N. Besides, the virtual impedance can be designed from 0.1 p.u. to 0.5 p.u, with a X/R ratio 10. Notably, as long as the GFM inverter system is small-signal stable, these control parameters are also possible to be designed beyond the above ranges. Even though, the power droop coefficients and virtual impedance are recommended to be designed within the above ranges, which can lower the risk of instability.

3.1.2. Multiple-Loop Grid-Forming Control Scheme

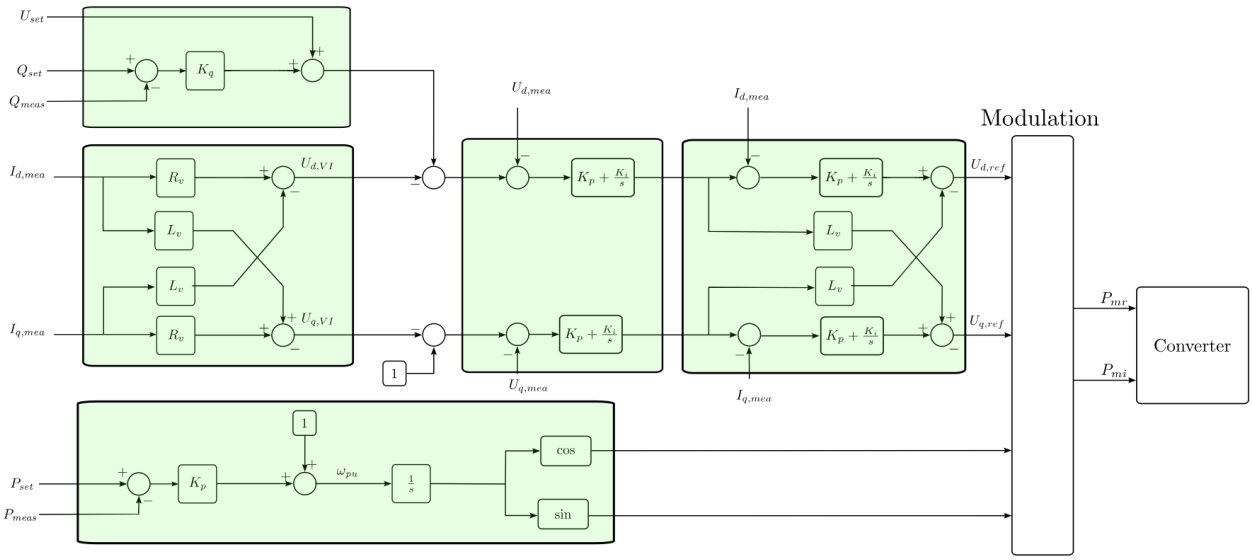

Figure 3.6: Multiple-loop grid-forming control scheme with virtual impedance.

The multiple-loop GFM control scheme with virtual impedance is presented in Figure 3.6. It includes not only active and reactive power controllers, but also the cascaded voltage and current controllers.

Similar to the single-loop GFM control scheme, the P-ω droop control is used to control the active power, and the Q-V droop control is used to control the reactive power, and a virtual impedance is used to enhance the stability of the GFM converter. However, different from the single-loop GFM control scheme, cascaded voltage and current PI controllers are included in the multiple-loop GFM control scheme in Figure 3.6. Adding the voltage and current PI controllers may increase the complexity of the control scheme, but it enables more accurate voltage and current control performance. Besides, the current limitation function is easier to implement in the multiple-loop GFM control scheme. For example, a simple way to limit the output current is by utilizing a current reference limiter.

Then, in terms of the control parameters of the multiple-loop GFM control scheme in Figure 3.6, the P and Q droop coefficients and the virtual impedance can be designed to be the same as that of the single-loop GFM control scheme in Figure 3.5. In order to have better control performance, the bandwidth of the inner current control loop should be designed as high as possible. Based on previous research experience, 1000 Hz can be used as an example. Besides, the bandwidth of the voltage control loop can be designed as 1/10 of current control loop's bandwidth, such as 100 Hz. Then, the PI parameters of the current controller and voltage controller can be designed accordingly.

Notably, the main study focus of Task 2.2 is the OEH, while the modelling and design of the offshore wind farms will be carried out by Task 3.2 in Work Package 3 (WP3). So, the detailed design of the offshore wind farms is not included in this report. Even though, in order to keep the completeness of the whole study system, a simplified aggregated offshore wind farm model will be briefly introduced in Section 4.1.

3.2. CONTROL DESIGN FOR THE DC HUB

After introducing the AC hub design, this section will focus on an offshore DC hub with an internal DC interconnector and two 2 GW HVDC systems. Figure 3.7 shows a general system configuration of the selected DC hub study case. The rated DC voltage of the DC hub is ±525 kV. The rated active power of

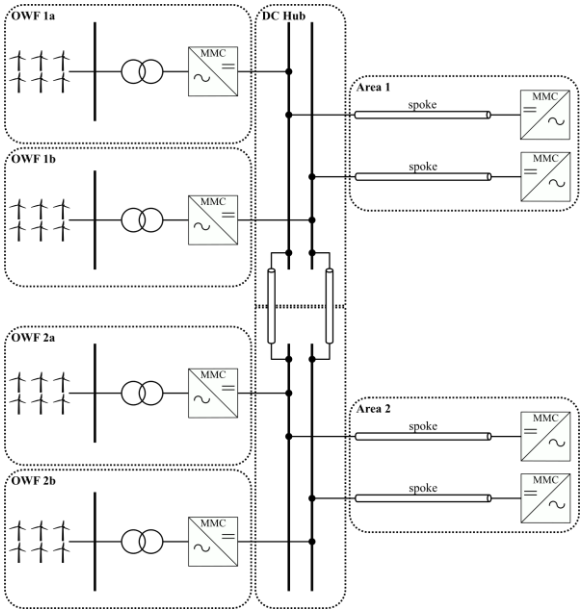

Figure 3.7: A general system configuration of the selected DC hub study case.

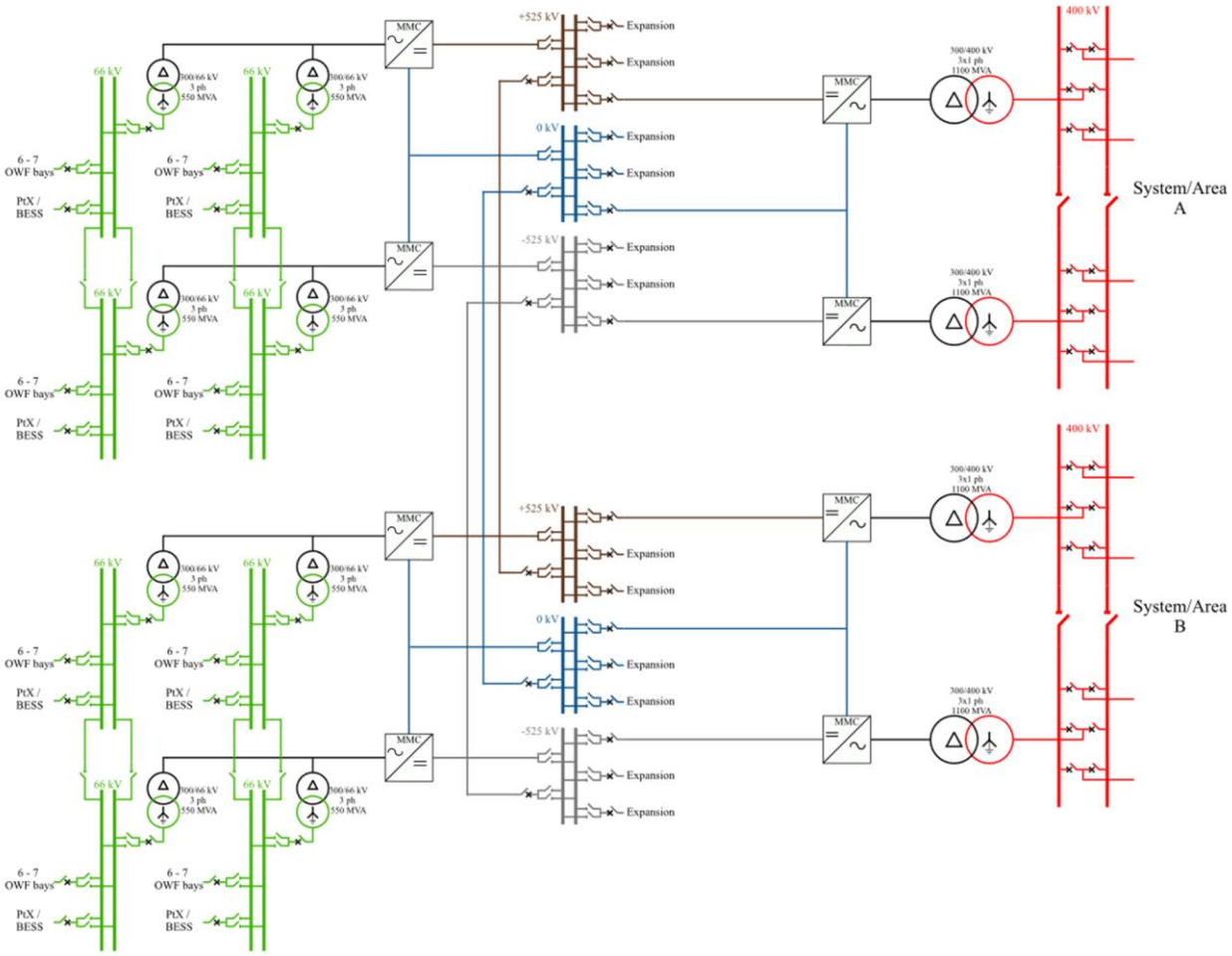

Figure 3.8: Detailed system configuration of the DC hub.

the two bipolar HVDC transmission systems is 2 GW. Moreover, offshore wind farms are connected to the offshore HVDC converter to inject power. In Figure 3.7, there are four offshore wind farms, and the rated power of each wind farm is 1 GW.

To be more specific, a more detailed system configuration of the selected DC hub study case is presented in Figure 3.8. The offshore wind farms are connected to 66 kV busbars, and three-phase Y-Δ transformers are used to connect the offshore wind farms and the offshore HVDC converter. The voltage ratio of the transformer is 66 kV/300 kV. Since the onshore HVDC converters are in charge of establishing the DC grid, the modelling and controller design of the onshore HVDC converters will be mainly discussed in the rest of Section 3.2.

3.2.1. Typical DC Voltage Control Scheme

As aforementioned, the main control target of the onshore HVDC converter is the DC voltage. So, a typical DC voltage control scheme is presented in Figure 3.9. It mainly includes an outer-loop controller for controlling the DC voltage (equivalent to controlling the active power) and an inner-loop controller

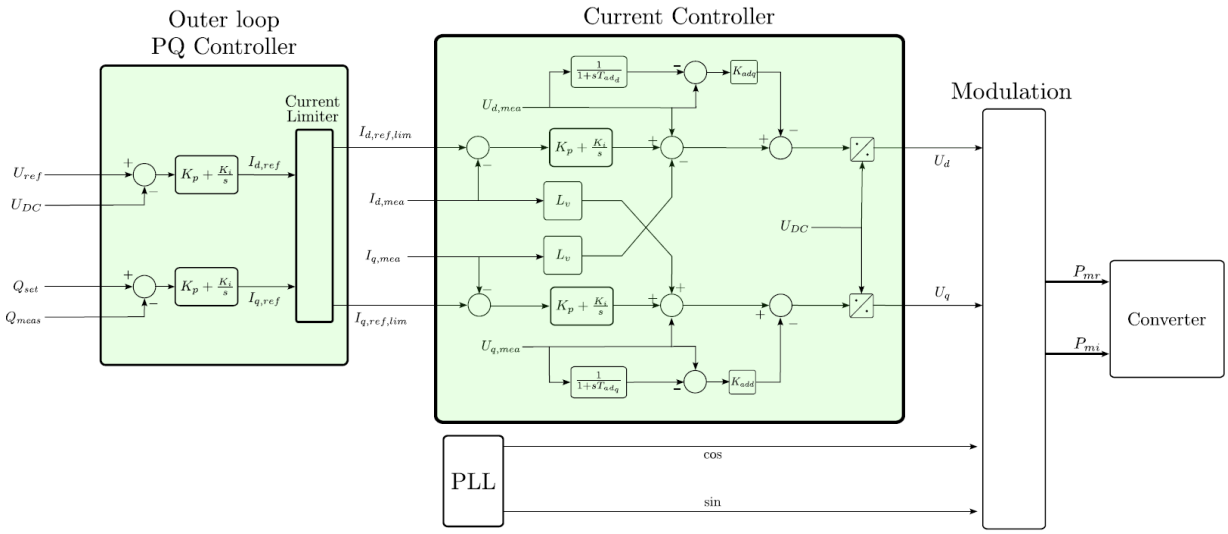

Figure 3.9: Typical DC voltage control scheme.

for controlling the AC current. To improve the dynamic performance, voltage feedforward is added to the current controller. Besides, a PLL is used to generate the angle for grid synchronization. This simple control structure enables an accurate DC voltage control by the onshore HVDC converter.

3.2.2. DC-Droop Control Scheme

In order to achieve stable operation and power sharing of the two onshore converters connected to the same DC system, the DC-droop control is necessary. From the literature, there are different possibilities to realise the DC-droop control, as such as V_{dc} - P_{ac} droop [12], P_{ac} - V_{dc} droop [13], V_{dc} - I_{dc} droop [14]. Among these options, the V_{dc} - P_{ac} droop control is selected, as it seems to be more straightforward than other methods.

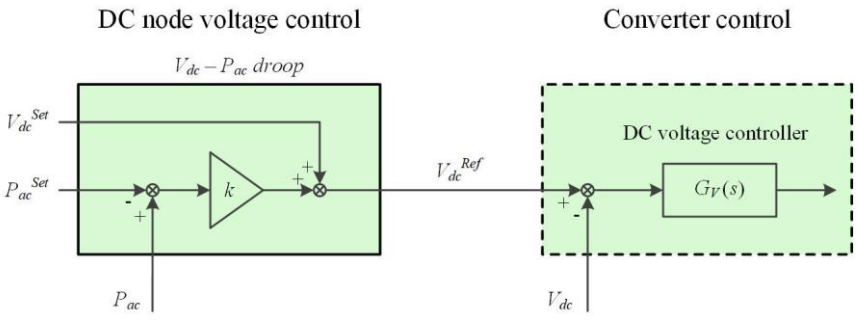

Figure 3.10: DC node droop control scheme [13].

The DC node droop control scheme is presented in Figure 3.10. It can be seen that the active power error goes through a droop controller at first. Then, it adds the DC voltage preset value to generate the DC voltage reference. Subsequently, the DC voltage reference is sent to the converter controller. The converter controls the DC voltage to be equal to the DC voltage reference. Notably, the detailed converter control scheme is shown in Figure 3.9, which is a grid-following control scheme with DC voltage control function.

4. PSCAD MODELLING AND SIMULATIONS

The power systems computer-aided design (PSCAD) is selected in this project as the primary simulation tool due to its powerful capabilities in modelling and analysing power systems with high accuracy and flexibility. It provides a user-friendly graphical interface that allows engineers to build detailed system models efficiently, while offering robust solvers for electromagnetic transient (EMT) simulations. Compared to other platforms, PSCAD excels in handling fast dynamic phenomena, such as switching events, fault transients, and power electronic interactions, which are critical for modern power systems. Its wide library of components, combined with the ability to customise models, makes it an industry-standard tool for both research and practical applications.

4.1. AC HUB MODEL DEVELOPMENT

The scope of the study in this section is building the EMT simulation model of the OEH. According to the system configuration of the AC hub presented in Figure 3.2, a simplified version of the AC hub model is built based on the PSCAD simulation platform, which is shown in Figure 4.1. Notably, considering the initial focus of the AC hub is the offshore AC grid, the onshore HVDC converter is ignored in the first version of the model. As shown in Figure 4.1, the first version AC hub model includes two offshore AC buses connected through an interconnector. On each offshore AC bus, four offshore wind farms (left side) and a bi-pole offshore HVDC converter (right side) are connected. The rated power of each offshore wind farm is 500 MW, while the rated power of the bi-pole offshore HVDC converter is 2 GW.

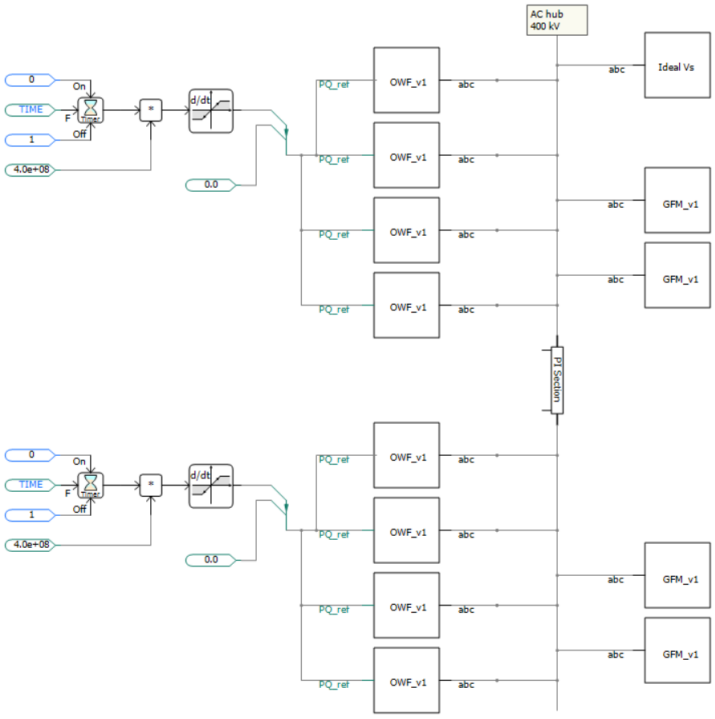

Figure 4.1: First version of the AC hub PSCAD model.

Figure 4.1 shows the general structure of the AC hub, more details about the sub-models (i.e., offshore wind farm and HVDC converter) are presented in Figures 4.2 and 4.3, where the offshore wind farm is controlled by the GFL method and the offshore HVDC converter is controlled by the GFM method.

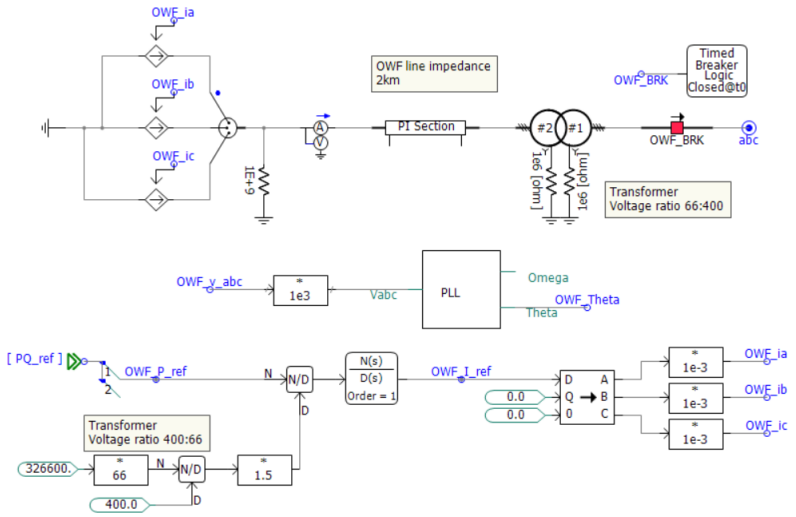

Figure 4.2: Simplified model of the offshore wind farm.

Figure 4.2 shows the detailed structure of the offshore wind farm model, which is a simplified and aggregated model. Specifically, the offshore wind turbine generator is simplified as a three-phase controlled current source with a PLL for voltage synchronization. Since all the offshore wind turbine generators are expected to connect to a 66 kV bus in realistic applications, a transformer is added between the wind farm and the AC hub to increase the voltage level from 66 kV to 400 kV. Notably, a 1 MΩ neutral earthing resistance is just selected as an example for the case study.

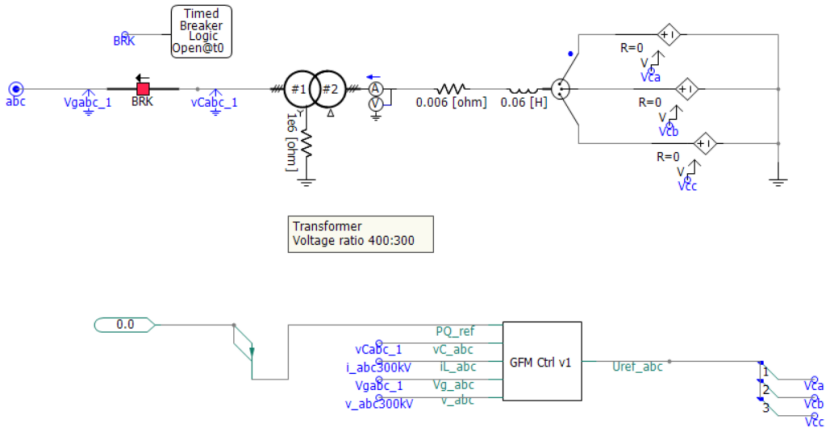

Figure 4.3: Simplified model of the offshore HVDC converter.

Figure 4.3 shows the detailed structure of the offshore HVDC converter, where an average-leg model is used to represent the HVDC converter. According to Figure 3.2, the rated voltage of the offshore HVDC converter is 300 kV. So, a transformer with a voltage ratio of 300 kV/400 kV is added between the HVDC converter and the AC hub. Considering the offshore grid voltage is usually built by the offshore HVDC converter, the offshore HVDC converter should be a GFM unit. As aforementioned, two widely used GFM control schemes are selected to study the performance of the AC hub, which are single-loop GFM control and multiple-loop GFM control. More details about GFM control will be introduced as follows.

4.1.1. SINGLE-LOOP GRID-FORMING CONTROL SCHEME

According to Figure 3.5, the single-loop GFM control scheme is modelled in PSCAD to control the offshore HVDC converter, which is shown in Figure 4.4. The 2.5% P-ω and 1% Q-V droop coefficients are selected as an example to study. Besides, for the single-loop GFM control, a virtual impedance with "X_v = 0.1 p.u. and R_v = 0.05 p.u." is used to enhance the small-signal stability.

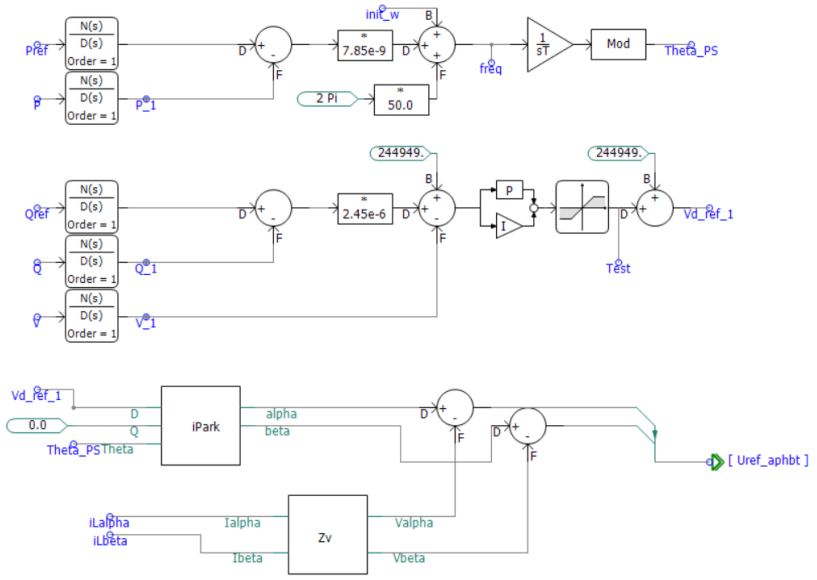

Figure 4.4: Single-loop grid-forming control model.

4.1.2. MULTIPLE-LOOP GRID-FORMING CONTROL SCHEME

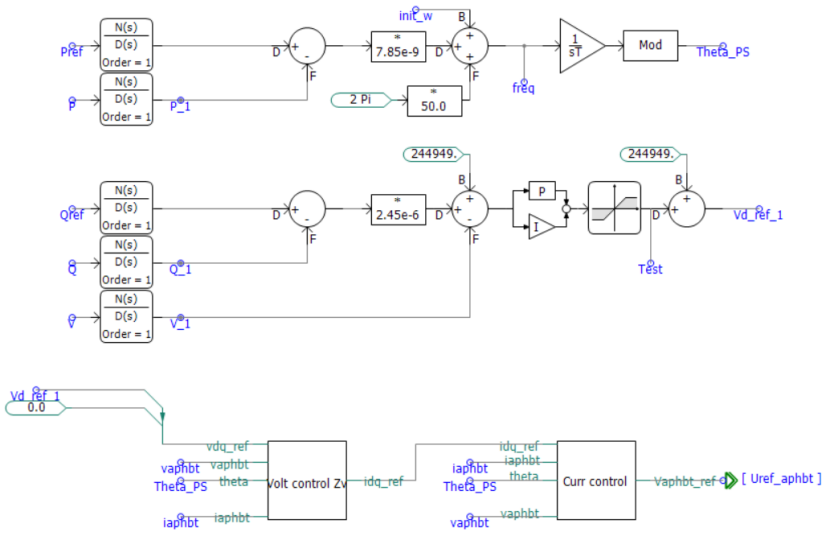

Figure 4.5: Multiple-loop grid-forming control model.

Moreover, according to Figure 3.6, the multiple-loop GFM control scheme is also modelled in PSCAD to control the offshore HVDC converter as an alternative control solution, which is shown in Figure 4.5. Similar to the single-loop GFM control scheme, the 2.5% P-ω and 1% Q-V droop coefficients are selected as an example to study. Different from the single-loop GFM control scheme, cascaded current and voltage PI controllers are used to control the current and voltage. Besides, a virtual impedance with "X_v = 0.4 p.u. and R_v = 0.04 p.u." is added to the voltage control to enhance the small-signal stability.

4.2. SIMULATIONS OF AC HUB IN DIFFERENT CASES

Following the modelling work, simulations under different scenarios will be carried out to evaluate the performance of the developed AC hub model. In this section, the simulation results of the AC hub with single-loop GFM control and multiple-loop GFM control under normal conditions will be presented. The scenarios include wind export, interarea power transfer, power step on wind farms, asymmetrical wind power generation, parameter sensitivity tests, etc. More details are introduced in this section.

4.2.1. SINGLE-LOOP GRID-FORMING CONTROL SCHEME

For the developed AC hub model with the single-loop GFM control scheme, six selected study cases under normal conditions are tested. It includes wind export, interarea power transfer, wind export plus interarea power transfer, power step change on wind farms, and asymmetrical wind power generation. The detailed active power distribution in each case is listed in Table 4.1.

Table 4.1: Selected study cases for the AC hub model

Study cases	Generated power by OWFs	Power through offshore HVDC converters
Case 1	OWF 1~4: 400 MW × 4	Offshore HVDC 1~2: -800 MW × 2
	OWF 5~8: 400 MW × 4	Offshore HVDC 3~4: -800 MW × 2
Case 2	OWF 1~4: 0 MW × 4	Offshore HVDC 1~2: +800 MW × 2
	OWF 5~8: 0 MW × 4	Offshore HVDC 3~4: -800 MW × 2
Case 3	OWF 1~4: 200 MW × 4	Offshore HVDC 1~2: +100 MW × 2
	OWF 5~8: 200 MW × 4	Offshore HVDC 3~4: -900 MW × 2
Case 4	OWF 1~4: 400 MW × 4	Offshore HVDC 1~2: -800 MW × 2
	OWF 5~8: 400 MW × 4	Offshore HVDC 3~4: -800 MW × 2
Case 5	OWF 1~4: 400 MW × 4	Offshore HVDC 1~2: -400 MW × 2
	OWF 5~8: 0 MW × 4	Offshore HVDC 3~4: -400 MW × 2
Case 6	OWF 1~4: 400 MW × 4	Offshore HVDC 1~2: -960 MW × 2
	OWF 5~8: 400 MW × 4	Offshore HVDC 3~4: -640 MW × 2

Study Case 1: Wind export

Figure 4.6 presents the developed AC hub PSCAD model operating in wind export scenarios, where each offshore wind farm generates 400 MW of active power and injects this power into the AC hub.

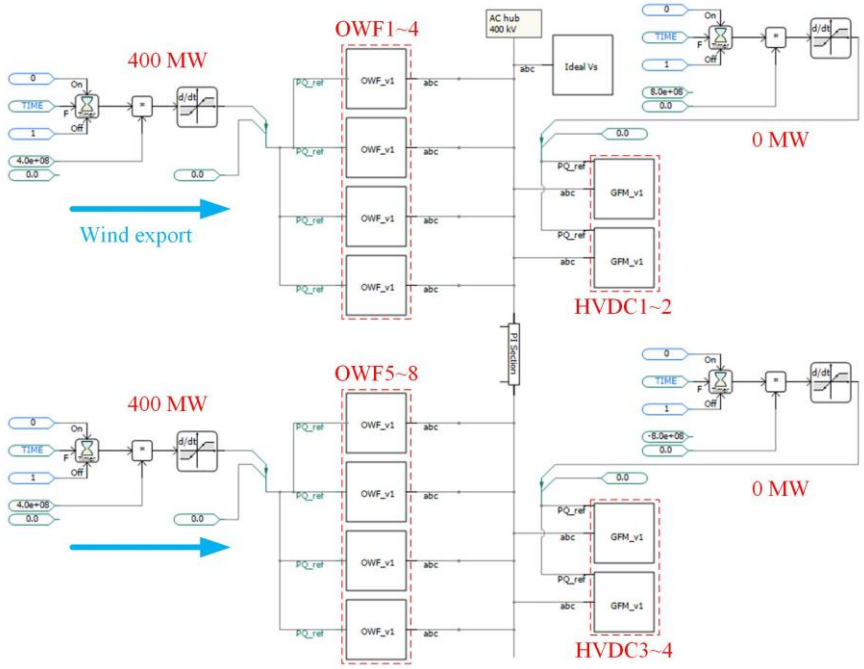

Figure 4.6: AC hub PSCAD model operating in wind export scenarios.

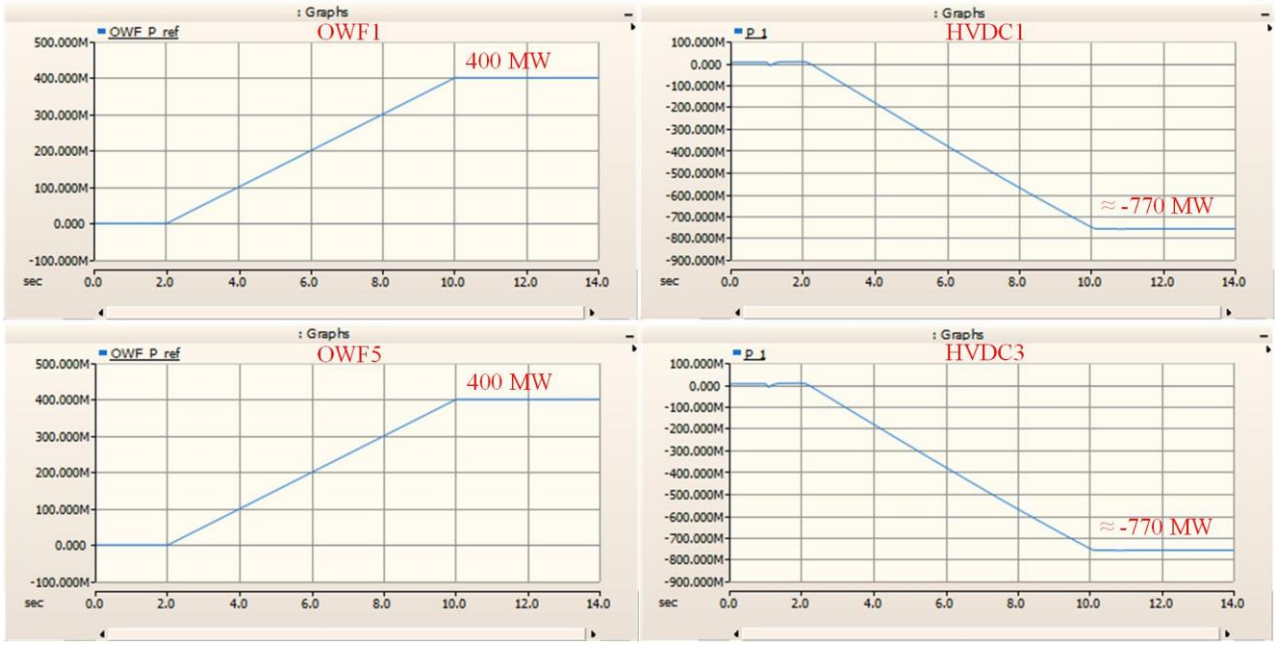

Figure 4.7: Simulation results of AC hub PSCAD model operating in wind export scenarios.

Figure 4.7 presents the simulation results of the AC hub PSCAD model operating in wind export scenarios. It can be seen that each offshore wind farm injects 400 MW of active power into the AC hub. Each HVDC converter absorbs nearly 800 MW of active power from the AC hub, demonstrating the capability to share power equally between HVDC converters. Notably, some power is lost on the 2 km transmission line (See Figure 4.2) and transformers as the parameters are not optimal, which needs further improvement in the future.

Study Case 2: Offshore converter power transfer

Figure 4.8 presents the developed AC hub PSCAD model operating in offshore converter power transfer scenarios, where the HVDC1~2 converter injects 800 MW of active power into the AC hub.

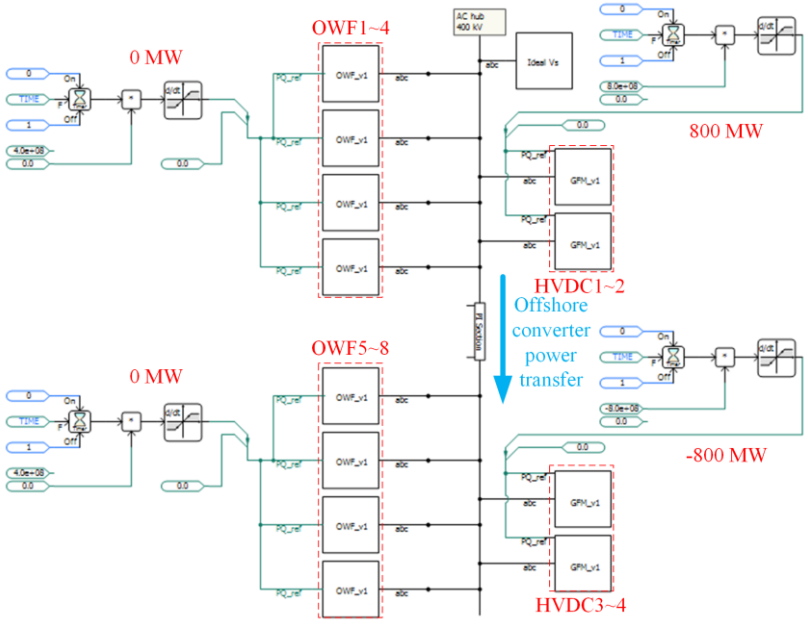

Figure 4.8: AC hub PSCAD model operating in offshore converter power transfer scenarios.

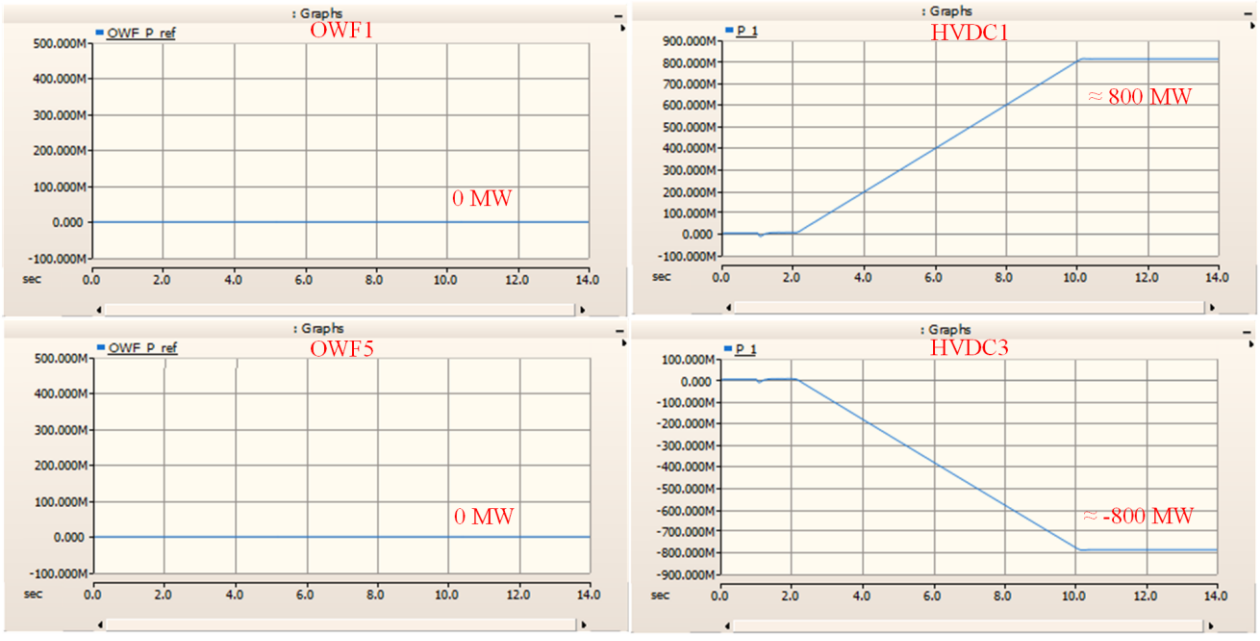

Figure 4.9: Simulation results of AC hub PSCAD model operating in offshore converter power transfer scenarios.

Figure 4.9 presents the simulation results of the AC hub PSCAD model operating in offshore converter power transfer scenarios. It can be seen that 800 MW of active power is transferred from the HVDC1~2 converter to the HVDC3~4 converter.

Study Case 3: Wind export plus offshore converter power transfer

Figure 4.10 presents the developed AC hub PSCAD model operating in wind export plus offshore converter power transfer scenarios, where each offshore wind farm injects 200 MW of active power into the AC hub and the HVDC1 converter injects around 500 MW of active power into the AC hub.

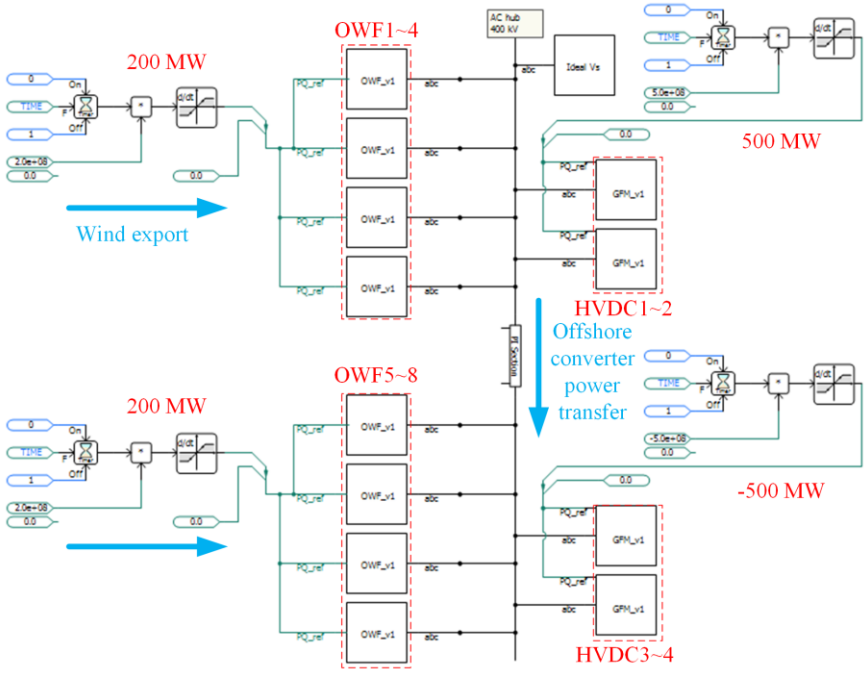

Figure 4.10: AC hub PSCAD model operating in wind export plus offshore converter power transfer scenarios.

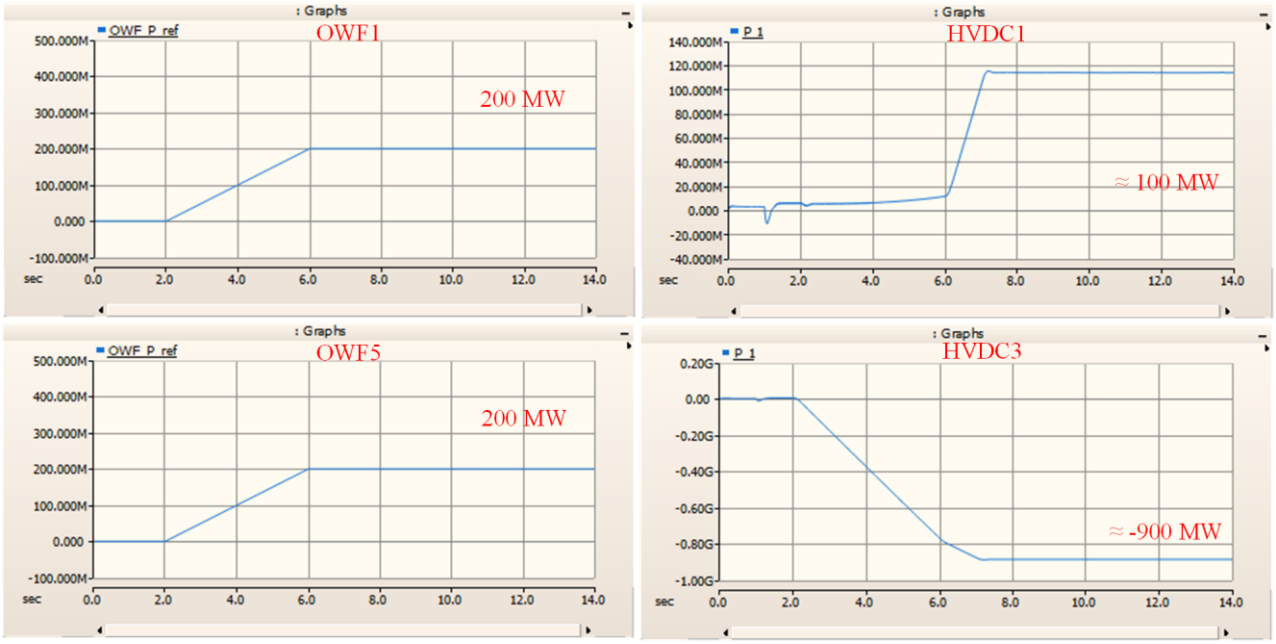

Figure 4.11: Simulation results of AC hub PSCAD model in wind export plus offshore converter power transfer scenarios.

Figure 4.11 presents the simulation results of the AC hub PSCAD model operating in wind export plus offshore converter power transfer scenarios. It can be seen that the HVDC1 converter injects around

100 MW of active power into the AC hub, and each wind farm injects 200 MW of active power. Then, the HVDC3 converter absorbs around 900 MW of the active power from the AC hub.

Study Case 4: Power step change on wind farms

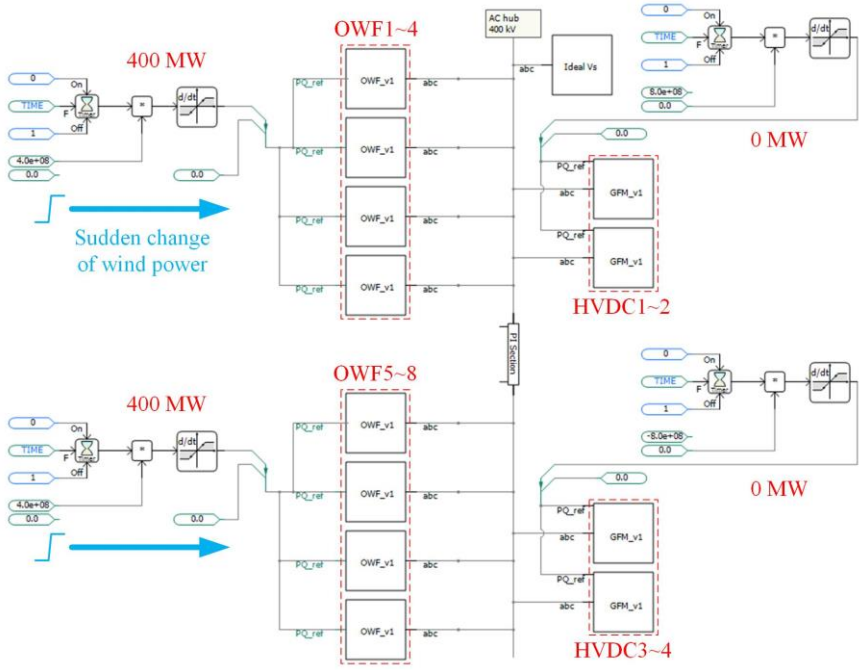

Figure 4.12: AC hub PSCAD model operating in sudden change of wind power scenarios.

Figure 4.12 presents the developed AC hub PSCAD model operating in sudden change of wind power scenarios, where each wind farm suddenly increases the output power from 0 to 400 MW. While this is an unrealistic scenario, it tests the capability of the controllers to adapt to active power changes in the desired way.

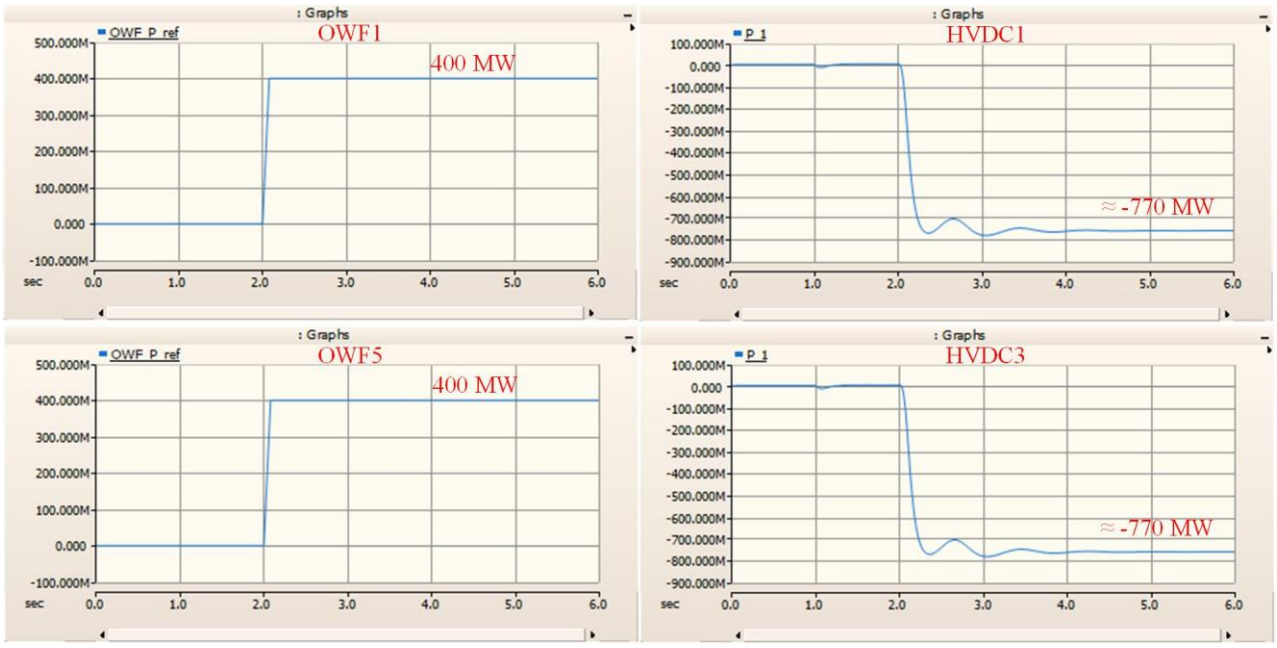

Figure 4.13: Simulation results of AC hub PSCAD model operating in sudden change of wind power scenarios.

Figure 4.13 presents the simulation results of the AC hub model operating in sudden change of wind power scenarios. It can be seen that the step response of the HVDC converters is fast. Besides, some oscillations appear during 2s-4s. In steady state, HVDC converters absorb around 770 MW of power.

Study Case 5: Asymmetrical wind power generation

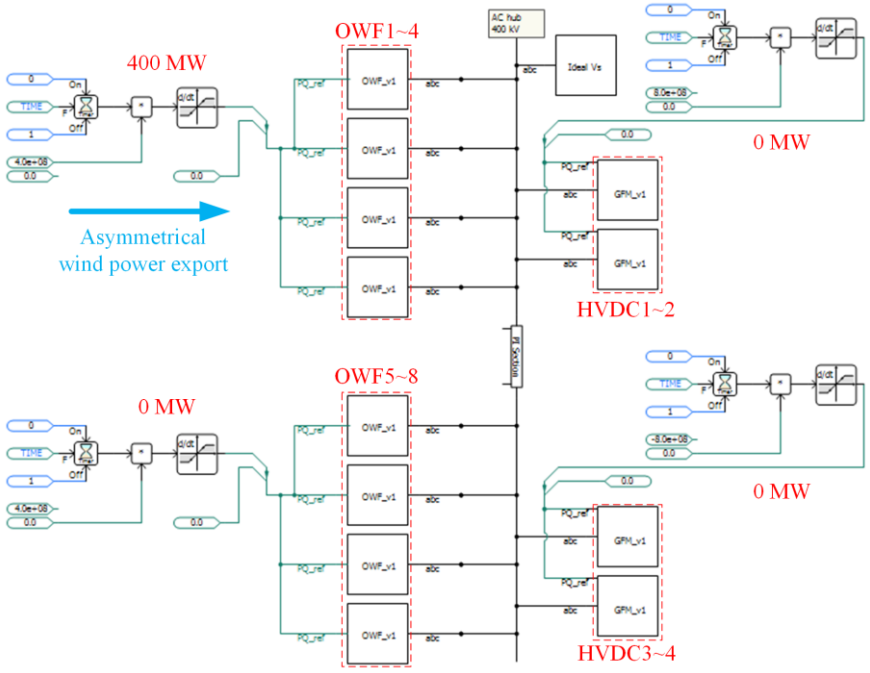

Figure 4.14: AC hub PSCAD model operating in asymmetrical wind power generation scenarios.

Figure 4.14 presents the developed AC hub PSCAD model operating in asymmetrical wind power generation scenarios, where wind farms 1~4 inject 400 MW of active power, while wind farms 5~8 inject zero power.

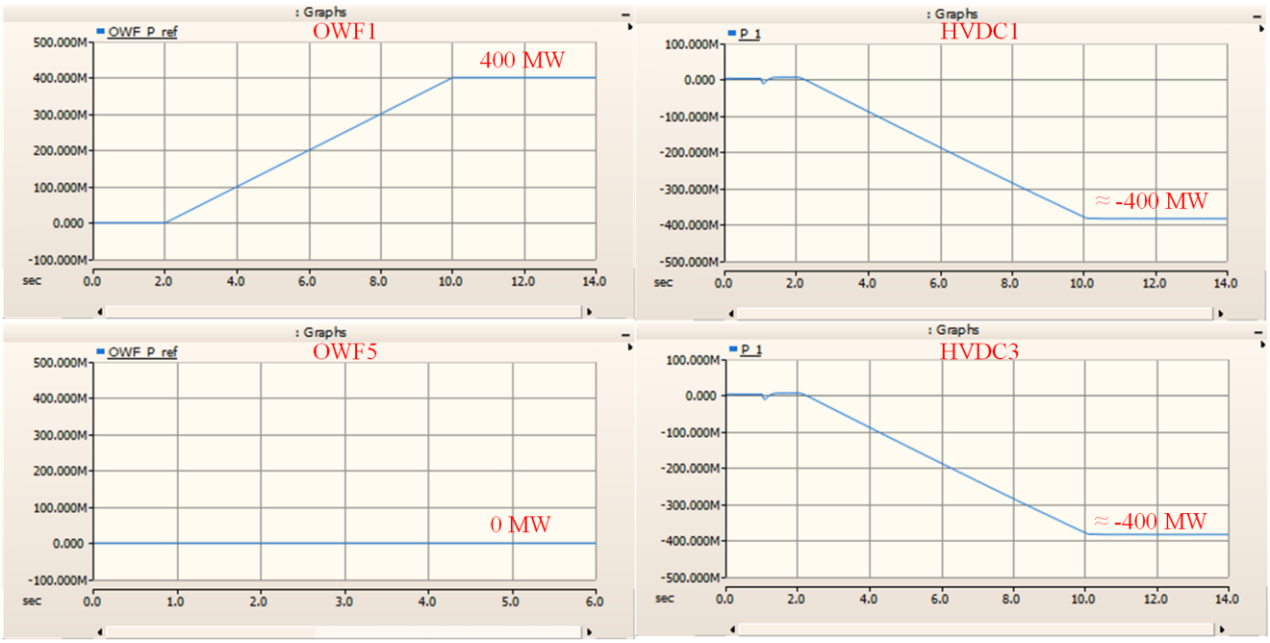

Figure 4.15: Simulation results of AC hub PSCAD model operating in asymmetrical wind power generation scenarios.

Figure 4.15 presents the simulation results of the AC hub PSCAD model operating in asymmetrical wind power generation scenarios. It can be seen that when each of the wind farms 1~4 injects 400 MW active power into the AC hub, the HVDC converters can share the active power from wind farms 1~4.

Study Case 6: HVDC converters with different droop coefficients

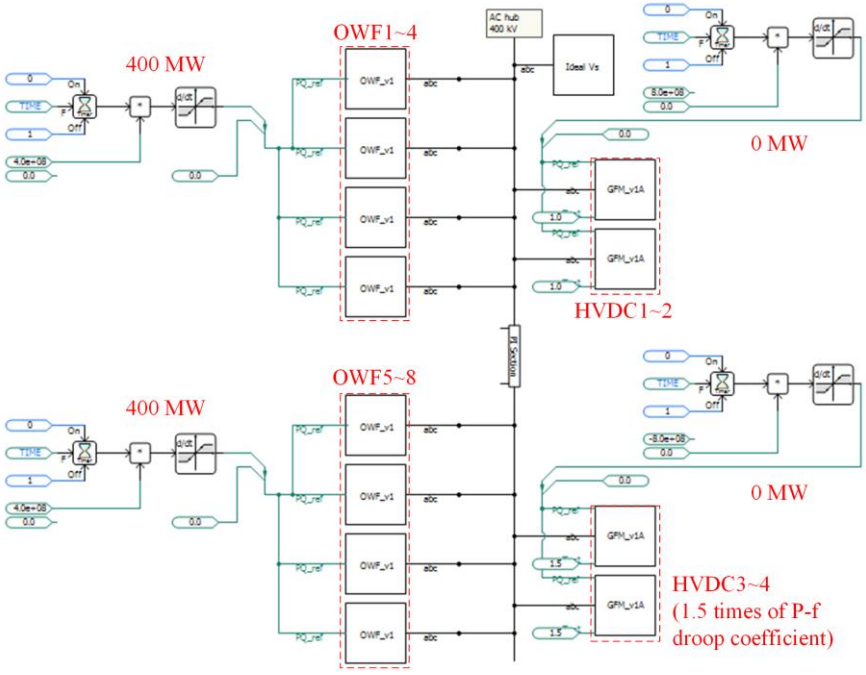

Figure 4.16: AC hub PSCAD model operating in HVDC converters with different droop coefficient scenarios.

Figure 4.16 presents the developed AC hub PSCAD model operating in HVDC converters with different droop coefficient scenarios, where the droop coefficient of HVDC3~4 is 1.5 times of the droop coefficient of HVDC1~2. Each wind farm injects 400 MW of active power to the hub.

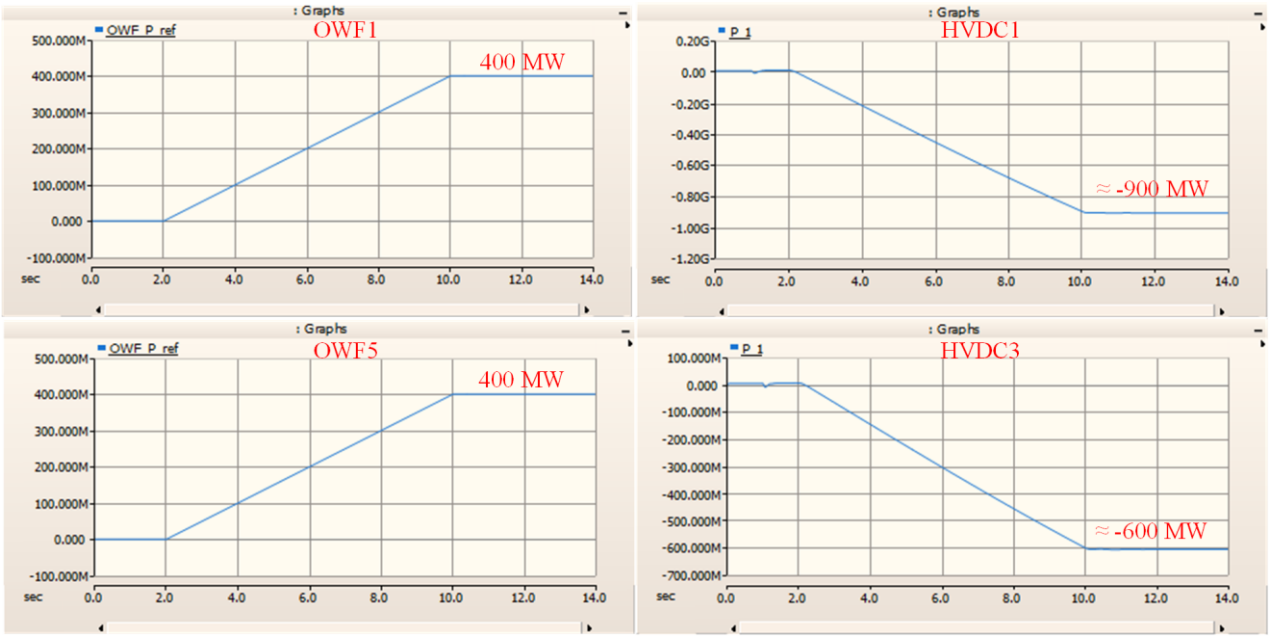

Figure 4.17: Simulation results of AC hub PSCAD model in HVDC converters with different droop coefficient scenarios.

Figure 4.17 presents the simulation results of the AC hub PSCAD model operating in HVDC converters with different droop coefficient scenarios. It can be seen that the HVDC converters 1~2 and HVDC converters 3~4 can share the active power according to the droop coefficients (i.e., 1:1.5).

4.2.2. Multiple-Loop Grid-Forming Control Scheme

The simulation results of the multiple-loop GFM control scheme will be illustrated as follows.

Study Case 1: Wind export

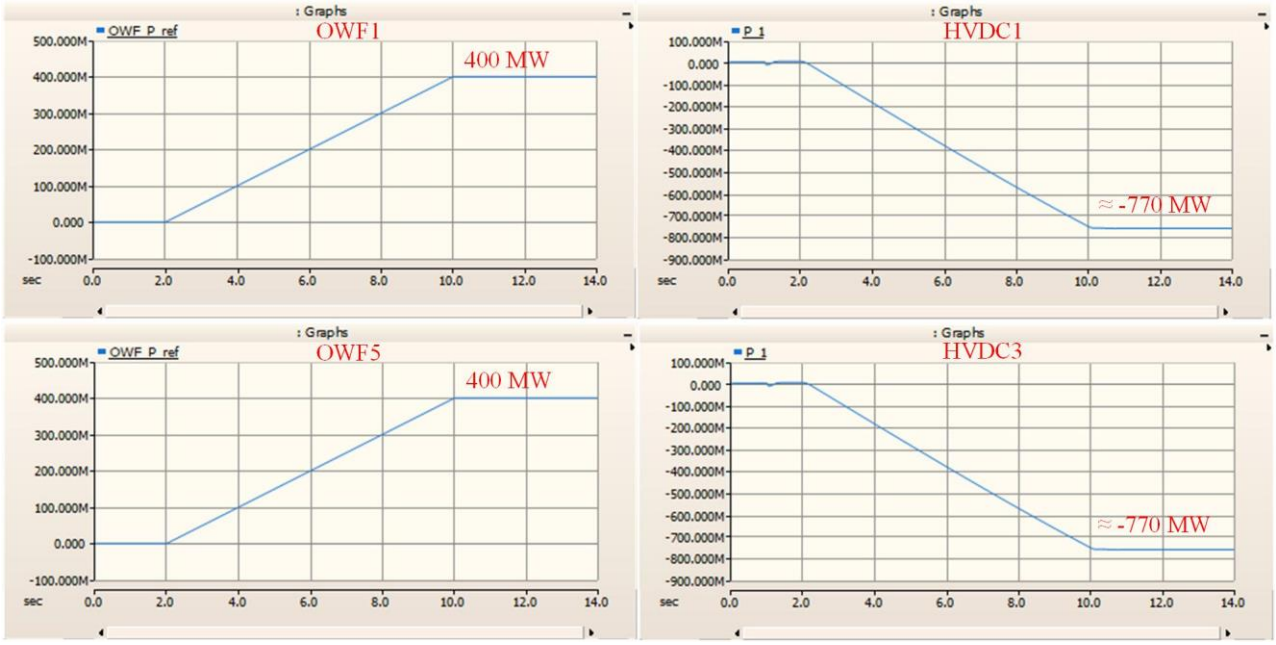

Figure 4.18: Simulation results of AC hub PSCAD model operating in wind export scenarios.

Study Case 2: Offshore converter power transfer

After replacing the single-loop GFM control scheme with the multiple-loop GFM control scheme for the developed AC hub PSCAD model, the simulation results in wind export scenarios are presented in Figure 4.18. The simulation results are highly similar to those of the single-loop GFM control scheme shown in Figure 4.7. Besides, Figure 4.19 presents the simulation results in offshore converter power transfer scenarios, which are similar to those of the single-loop GFM control scheme in Figure 4.9.

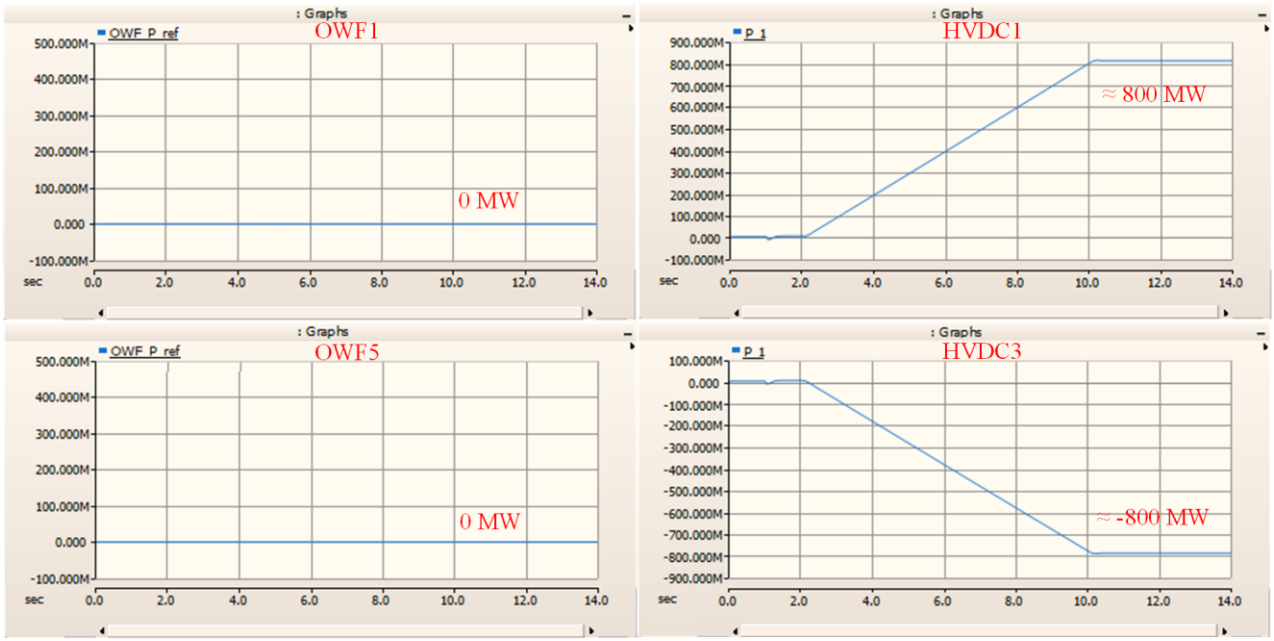

Figure 4.19: Simulation results of AC hub PSCAD model operating in offshore converter power transfer scenarios.

Study Case 3: Wind export together with offshore converter power transfer

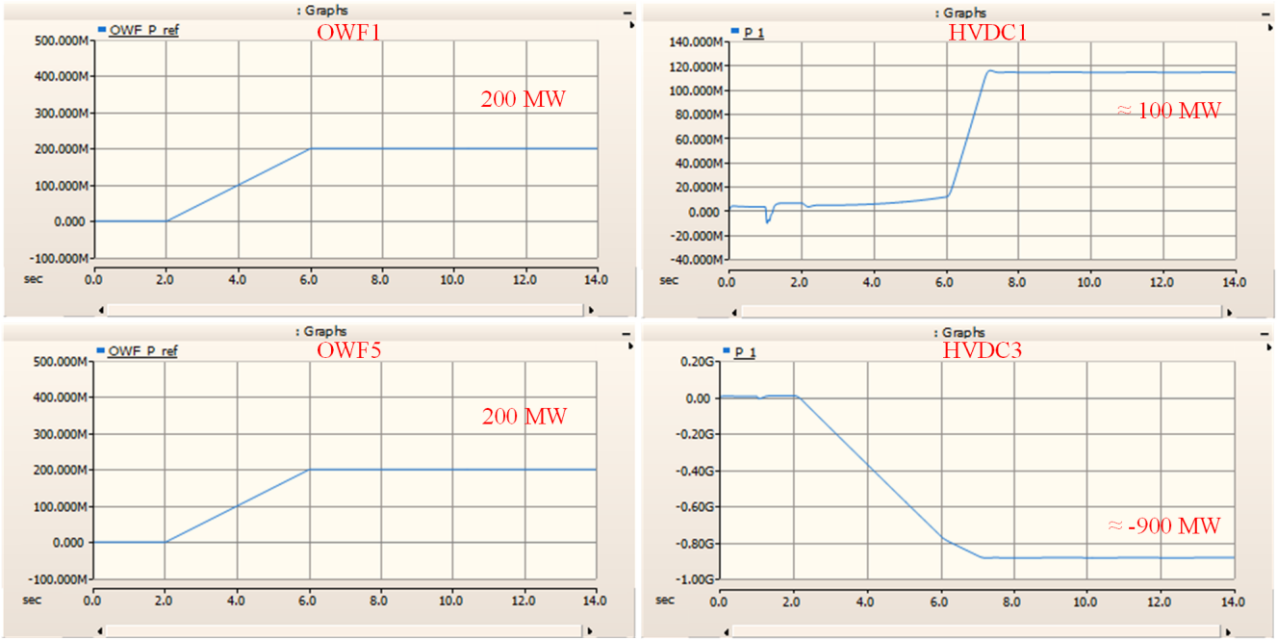

Figure 4.20: Simulation results of AC hub PSCAD model in wind export plus offshore converter power transfer scenarios.

Figure 4.20 presents the simulation results by using the multiple-loop GFM control scheme in wind export plus offshore converter power transfer scenarios, where the study case is the same as Figure 4.10. It can be seen that the HVDC1 converter injects around 100 MW of active power into the AC hub, and each wind farm injects 200 MW of active power. Then, the HVDC3 converter absorbs around 900 MW of the active power from the AC hub. The simulation results are highly similar to those of the single-loop GFM control scheme shown in Figure 4.11.

It is worth mentioning that when the total power of the HVDC is higher than 1000 MW, the current limiter will be triggered, and it may cause instability issues. However, the current limiting methods of the GFM inverter are highly relevant to the transient instability issues under fault conditions. So, these situations need to be considered when developing effective overcurrent protection methods for the GFM inverter. This work will be carried out in the next stage (i.e., GFM inverters operating under abnormal conditions).

Study Case 4: Power step change on wind farms

Figure 4.21 presents the simulation results by using the multiple-loop GFM control scheme in sudden change of wind power scenarios, where the study case is the same as Figure 4.12. It can be seen that after the sudden increase of wind power, the HVDC converters can absorb the active power from the AC hub as fast as possible. In the steady state, each HVDC converter absorbs around 770 MW of power. These simulation results are similar to those of the single-loop GFM control scheme shown in Figure 4.13.

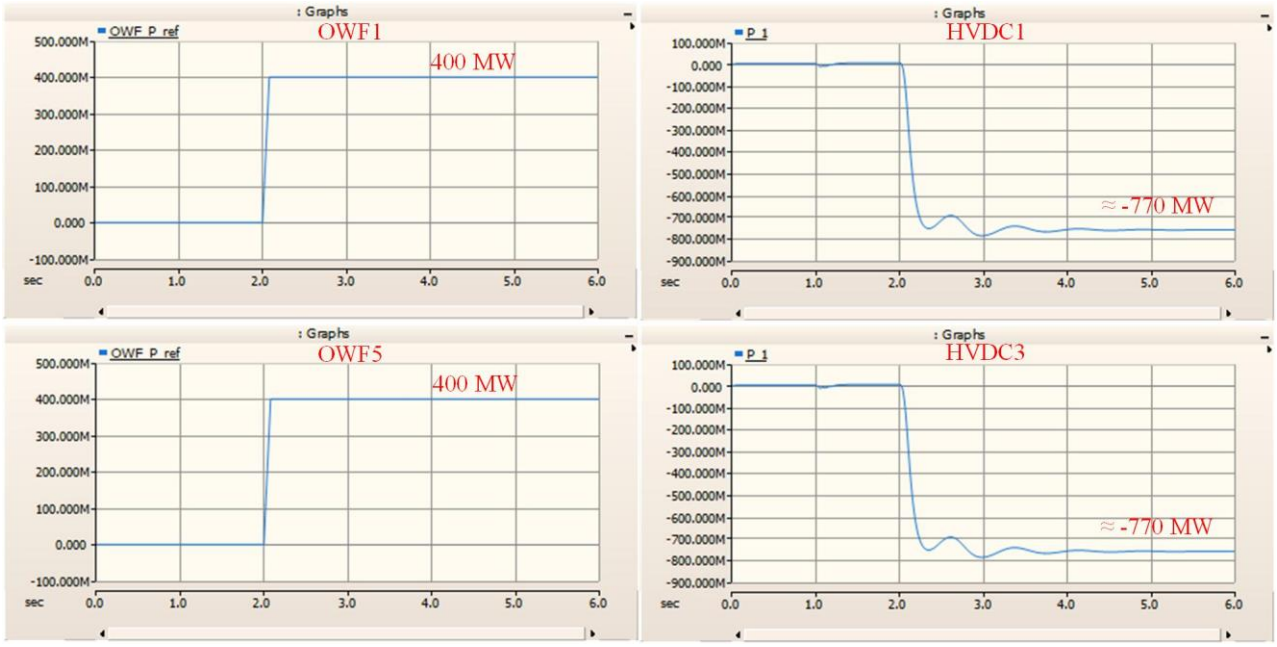

Figure 4.21: Simulation results of AC hub PSCAD model operating in sudden change of wind power scenarios.

Study Case 5: Asymmetrical wind power generation

Figure 4.22 presents the simulation results by using the multiple-loop GFM control scheme in asymmetrical wind power generation scenarios, where the study case is identical to Figure 4.14. It can be seen from Figure 4.22 that when each of the wind farms 1~4 injects 400 MW active power into the AC hub, the HVDC converters can share this active power due to the P-f droop control. These simulation results are similar to those of the single-loop GFM control scheme shown in Figure 4.15.

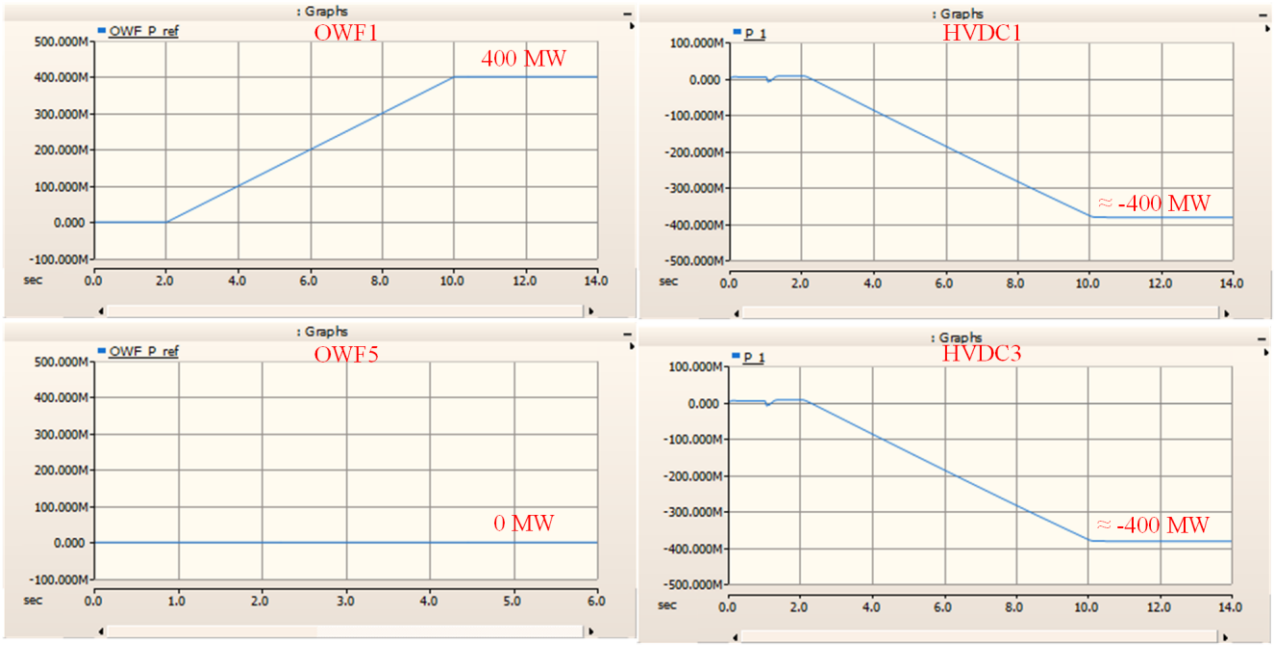

Figure 4.22: Simulation results of AC hub PSCAD model operating in asymmetrical wind power generation scenarios.

Study Case 6: HVDC converters with different droop coefficients

Figure 4.23 presents the simulation results of the AC hub PSCAD model operating in HVDC converters with different droop coefficient scenarios. It can be seen that the HVDC converters 1~2 and HVDC converters 3~4 can share the active power according to the droop coefficients (i.e., 1:1.5). These simulation results are similar to those of the single-loop GFM control scheme shown in Figure 4.17.

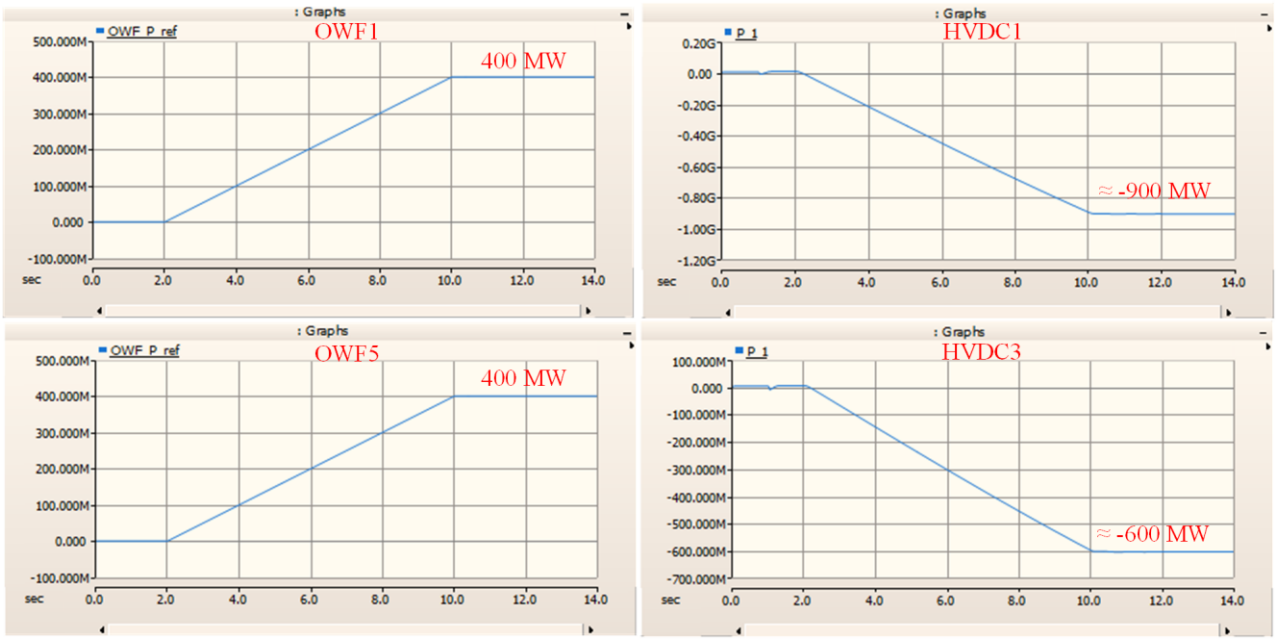

Figure 4.23: Simulation results of AC hub PSCAD model in HVDC converters with different droop coefficient scenarios.

Overall, the above simulation results indicate that the developed AC hub PSCAD model with both the single-loop and the multiple-loop GFM control schemes works well and as expected in steady-state and for relevant dynamic events (excluding faults) in the selected six cases. Besides, it is worth

mentioning that when the onshore HVDC converters shown in Figure 3.2 are included in the AC hub model, the simulation results of the offshore wind farms and offshore HVDC converters are still the same. More details about the developed onshore HVDC converter will be introduced in Section 4.3.

4.3. DC HUB MODEL DEVELOPMENT

Following the AC hub model development, the DC hub model is developed further. According to the system configuration of the DC hub presented in Figure 3.8, a DC hub model is built based on the PSCAD simulation platform, which is shown in Figure 4.24. It can be seen that for the DC hub case, the two HVDC systems are connected on the DC side. A transformer with a voltage ratio of 300 kV/400 kV is placed between the onshore HVDC converter and the onshore grid. Besides, each four offshore wind farms are connected to a bi-pole offshore HVDC converter. The rated power of each offshore wind farm is 500 MW, while the rated power of the bi-pole offshore HVDC converter is 2 GW.

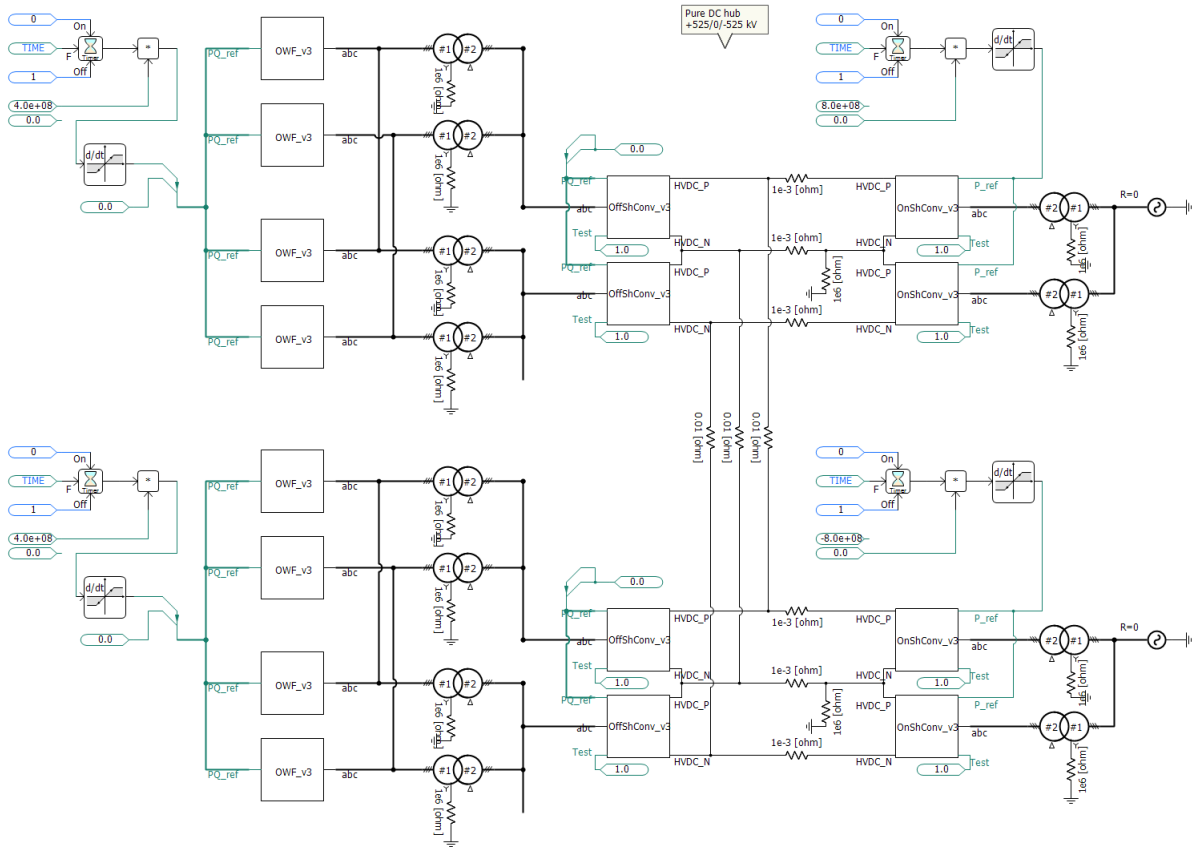

Figure 4.24: DC hub PSCAD model.

Figure 4.25 shows the detailed structure of the onshore HVDC converter. It can be seen from Figure 4.25 that an average-leg model is used to represent the onshore HVDC converter. Besides, the same amount of active power links the DC side and the AC side in the average model of the HVDC converter. Regarding the control scheme, the DC voltage control scheme shown in Figures 3.9 and the DC node droop control scheme shown in Figure 3.10 are used to control the DC voltage. A 5% V_{dc}-P_{ac} droop coefficient is selected as an example for analysis.

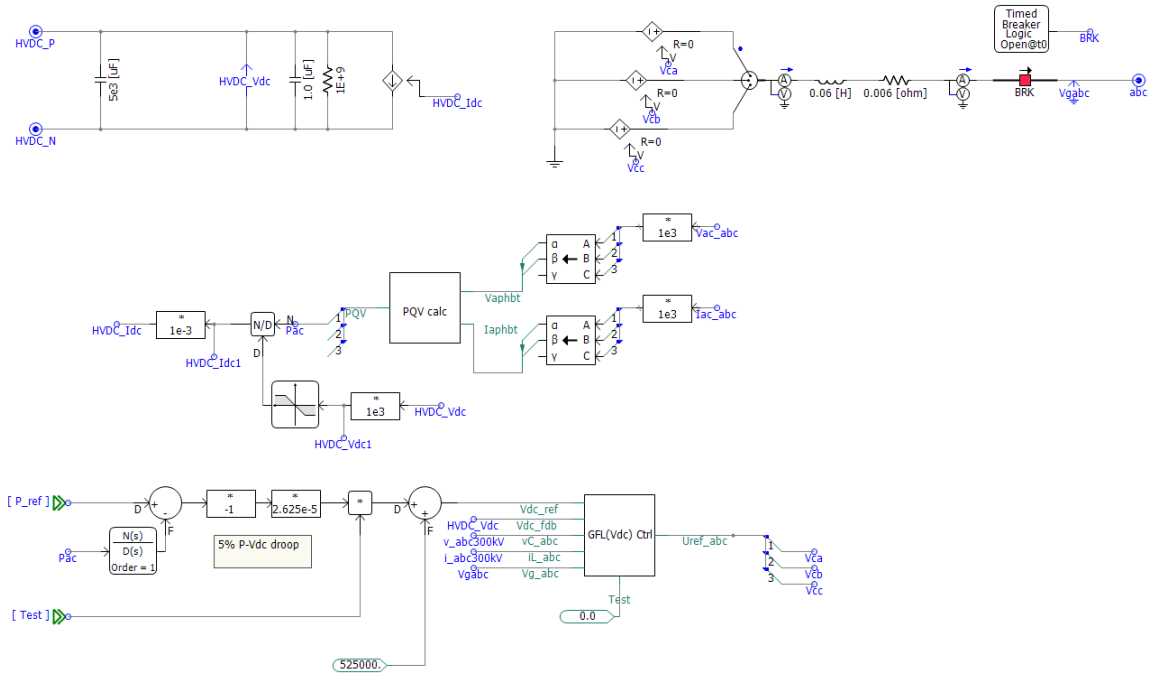

Figure 4.25: Average model of the onshore HVDC converter with DC droop control.

4.4. SIMULATIONS OF DC HUB IN DIFFERENT CASES

Based on the developed DC hub PSCAD model shown in Figure 4.24, simulations under different scenarios are carried out to evaluate the performance of the developed DC hub model. In this section, the simulation results of the DC hub with DC droop control under normal conditions will be presented. The selected test scenarios include wind export, interarea power transfer, power step on wind farms, asymmetrical power generation from two wind farm areas, asymmetrical power generation from one wind farm area, asymmetrical power from bi-pole HVDC onshore converter, and parameter sensitivity tests. The detailed active power distribution in each case is listed in Table 4.2.

Table 4.2: Selected study cases for the DC hub model

Study cases	Generated power by OWFs	Power through offshore HVDC converters	Power through onshore HVDC converters
Case 1	OWF 1~4: 400 MW × 4	Off-HVDC 1~2: -800 MW × 2	On-HVDC 1~2: 800 MW × 2
	OWF 5~8: 400 MW × 4	Off-HVDC 3~4: -800 MW × 2	On-HVDC 3~4: 800 MW × 2
Case 2	OWF 1~4: 0 MW × 4	Off-HVDC 1~2: 0 MW × 2	On-HVDC 1~2: +400 MW × 2
	OWF 5~8: 0 MW × 4	Off-HVDC 3~4: 0 MW × 2	On-HVDC 3~4: -400 MW × 2
Case 3	OWF 1~4: 200 MW × 4	Off-HVDC 1~2: -400 MW × 2	On-HVDC 1~2: +900 MW × 2
	OWF 5~8: 200 MW × 4	Off-HVDC 3~4: -400 MW × 2	On-HVDC 3~4: -100 MW × 2
Case 4	OWF 1~4: 400 MW × 4	Off-HVDC 1~2: -800 MW × 2	On-HVDC 1~2: 800 MW × 2
	OWF 5~8: 400 MW × 4	Off-HVDC 3~4: -800 MW × 2	On-HVDC 3~4: 800 MW × 2
Case 5A	OWF 1~4: 400 MW × 4	Off-HVDC 1~2: -800 MW × 2	On-HVDC 1~2: 400 MW × 2
	OWF 5~8: 0 MW × 4	Off-HVDC 3~4: 0 MW × 2	On-HVDC 3~4: 400 MW × 2
Case 5B	OWF 1,2,5,6: 400 MW × 4	Off-HVDC 1~2: -400 MW × 2	On-HVDC 1~2: 400 MW × 2
	OWF 3,4,7,8: 0 MW × 4	Off-HVDC 3~4: -400 MW × 2	On-HVDC 3~4: 400 MW × 2
Case 6	OWF 1~4: 0 MW × 4	Off-HVDC 1~2: 0 MW × 2	On-HVDC 1: 400 MW
	OWF 5~8: 0 MW × 4	Off-HVDC 3~4: 0 MW × 2	On-HVDC 3: -400 MW
Case 7	OWF 1~4: 400 MW × 4	Off-HVDC 1~2: -800 MW × 2	On-HVDC 1~2: 960 MW × 2
	OWF 5~8: 400 MW × 4	Off-HVDC 3~4: -800 MW × 2	On-HVDC 3~4: 640 MW × 2

Study Case 1: Wind export

Figure 4.26 presents the developed DC hub PSCAD model operating in wind export scenarios, where each offshore wind farm generates 400 MW of active power and injects this power into the DC hub through the offshore HVDC converters. The total power in the DC hub is absorbed by two onshore HVDC converters equally.

The simulation results of the DC hub PSCAD model operating in wind export scenarios are presented in Figure 4.27. It can be seen that each wind farm (such as OWF1 and OWF5) generates 400 MW of active power. The power is transferred to offshore HVDC converters, where the offshore HVDC converters 1 and 3 have 800 MW, respectively. Then, the power is further transferred to onshore HVDC converters, where the onshore HVDC converters 1 and 3 have 800 MW, respectively. Finally, the power is transferred to the onshore grids.

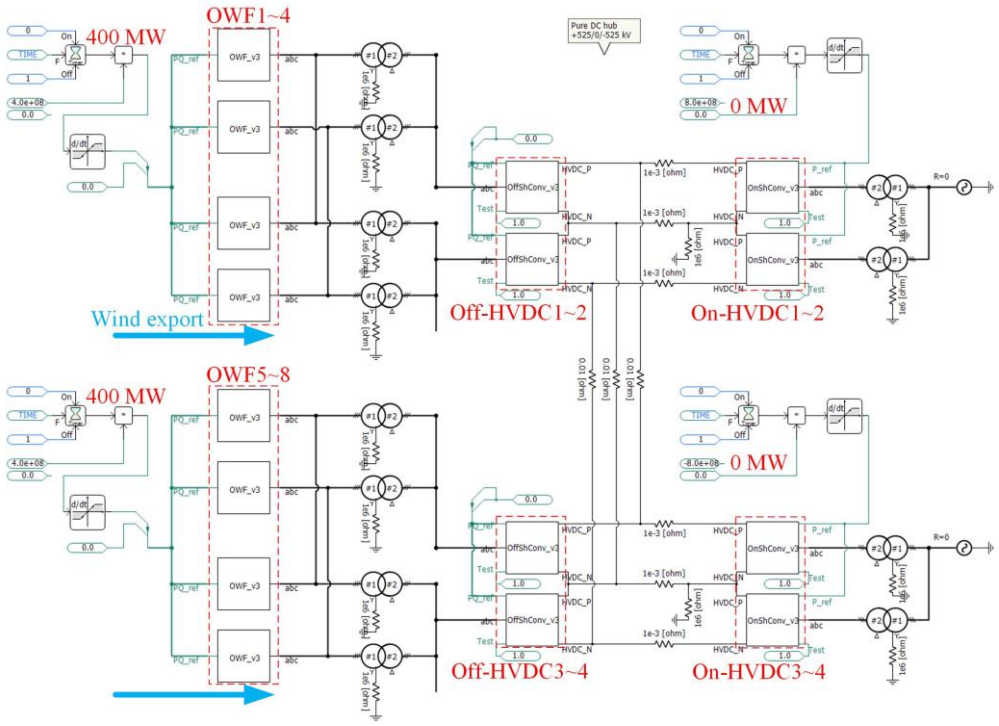

Figure 4.26: DC hub PSCAD model operating in wind export scenarios.

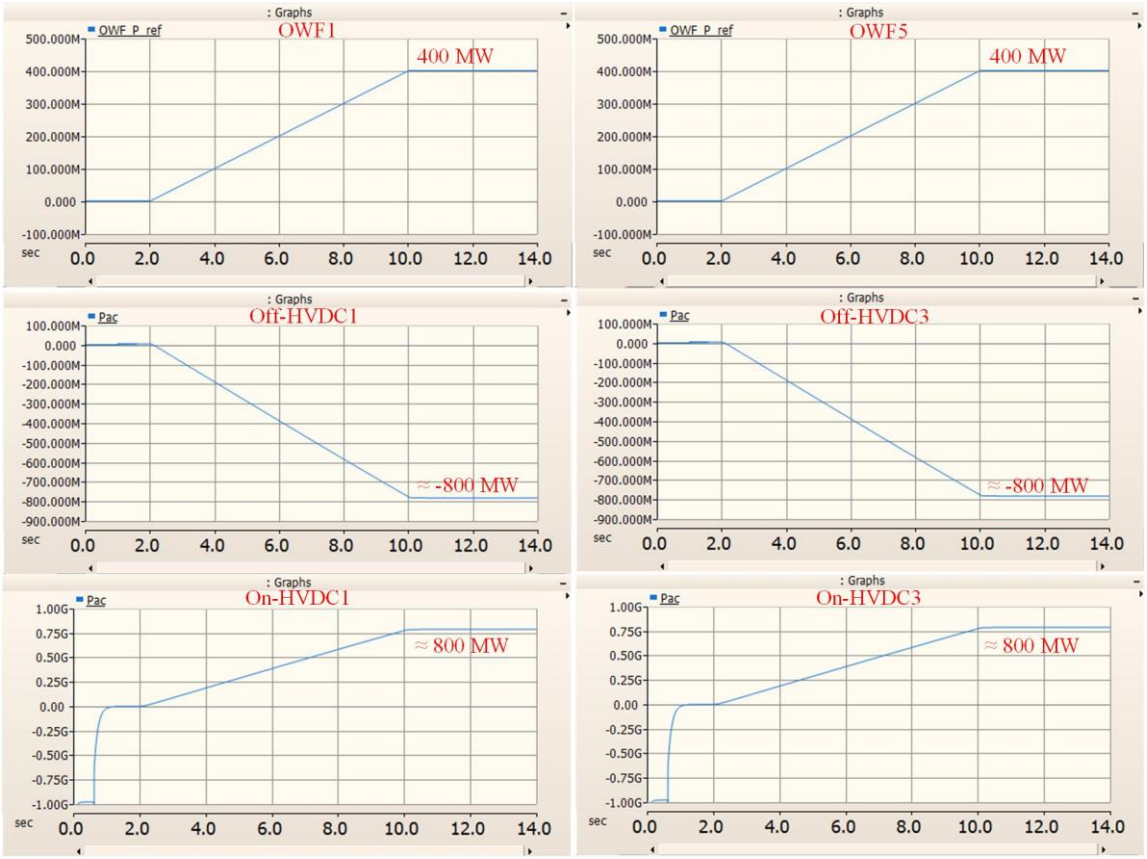

Figure 4.27: Simulation results of the DC hub PSCAD model operating in wind export scenarios.

Study Case 2: Interarea power transfer

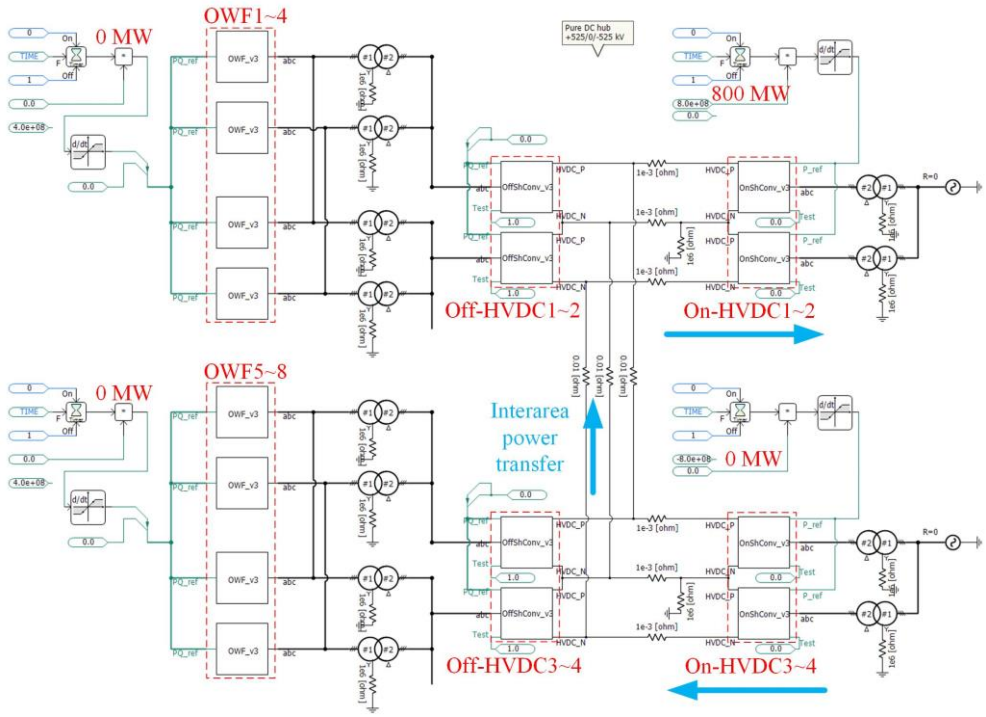

Figure 4.28: DC hub PSCAD model operating in interarea power transfer scenarios.

Figure 4.28 presents the developed DC hub PSCAD model operating in interarea power transfer scenarios. In this case, each wind farm does not generate any power. But the power flow goes from one onshore area to another through the DC hub.

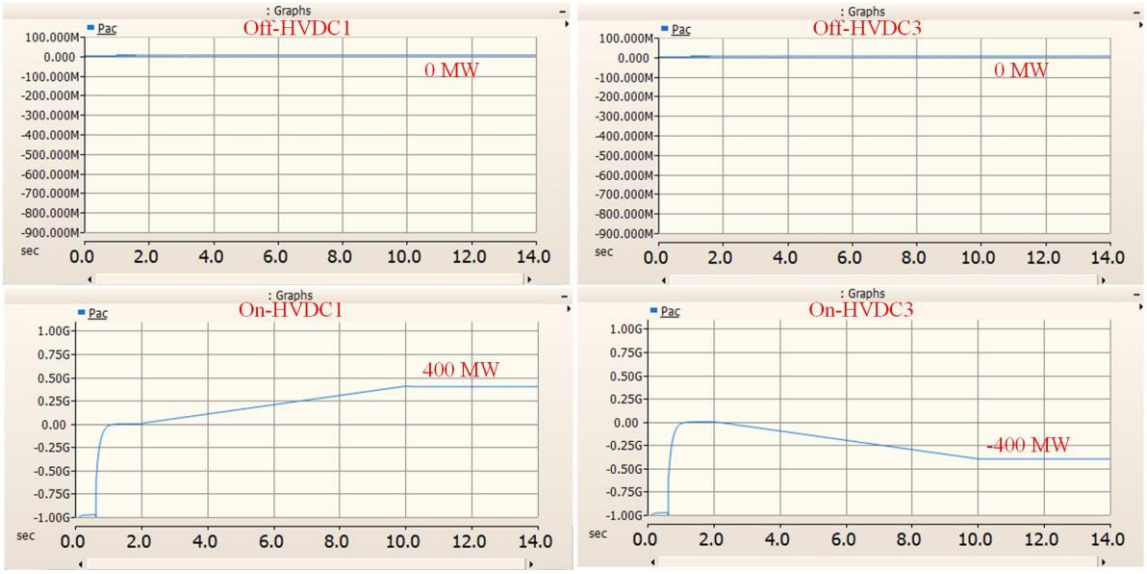

Figure 4.29: Simulation results of the DC hub PSCAD model operating in interarea power transfer scenarios.

The simulation results of the DC hub PSCAD model operating in interarea power transfer scenarios are presented in Figure 4.29. It can be seen that 400 MW per pole of active power is transferred from one area to another area through the onshore HVDC converters 3 and 1.

Study Case 3: Wind export plus interarea power transfer

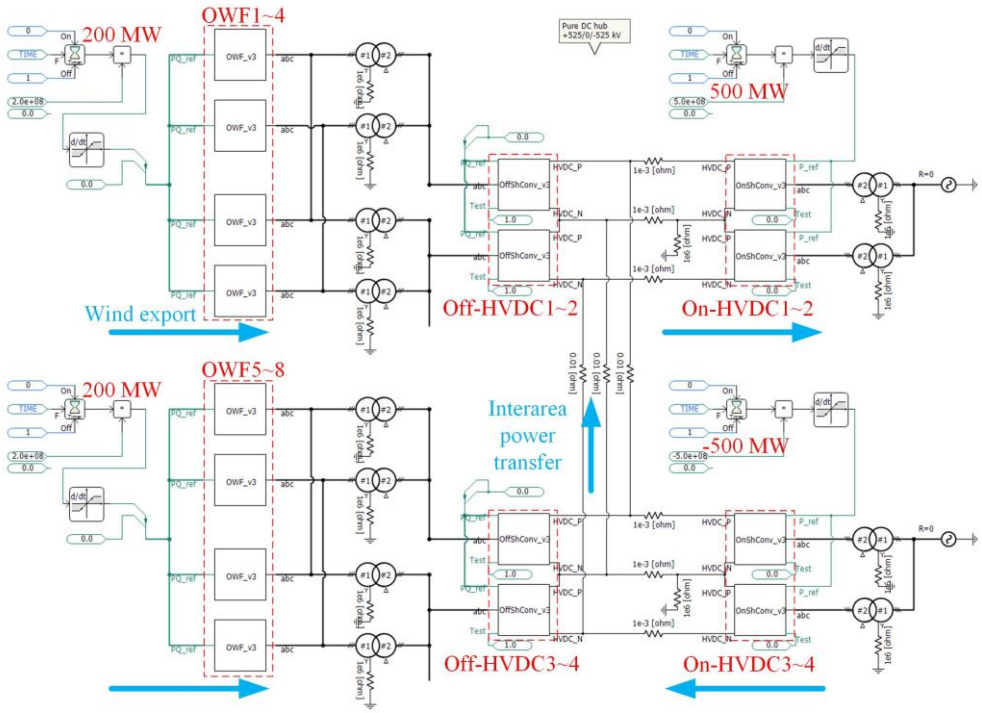

Figure 4.30: DC hub PSCAD model operating in wind export plus interarea power transfer scenarios.

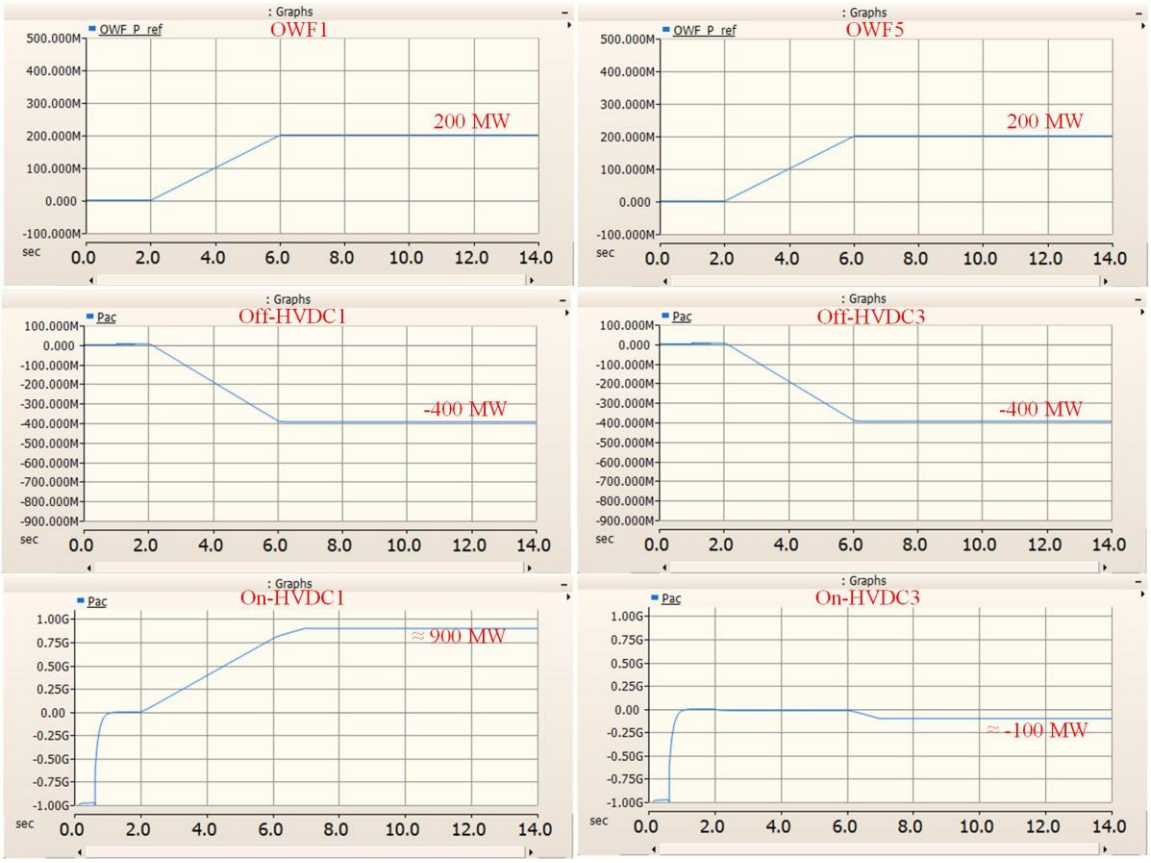

Figure 4.31: Simulation results of the DC hub PSCAD model operating in wind export plus interarea power transfer scenarios.

Figure 4.30 presents the developed DC hub PSCAD model operating in wind export plus interarea power transfer scenarios. In this case, each offshore wind farm generates 200 MW of active power and injects this power into the DC hub through the offshore HVDC converters. On the other hand, the onshore HVDC converters 3 and 4 also inject a certain amount of power into the DC hub. All the power in the DC hub is transferred to the HVDC converters 1 and 2.

The simulation results of the DC hub PSCAD model operating in wind export plus interarea power transfer scenarios are presented in Figure 4.31. It can be seen that 400 MW of active power is transferred from the offshore HVDC converters 1 and 3 to the DC hub, respectively. Meanwhile, 100 MW of active power is transferred from the onshore HVDC converter 3 to the DC hub. Finally, the power in the DC hub is transferred to the onshore HVDC converter 1.

Study Case 4: Power step on wind farms

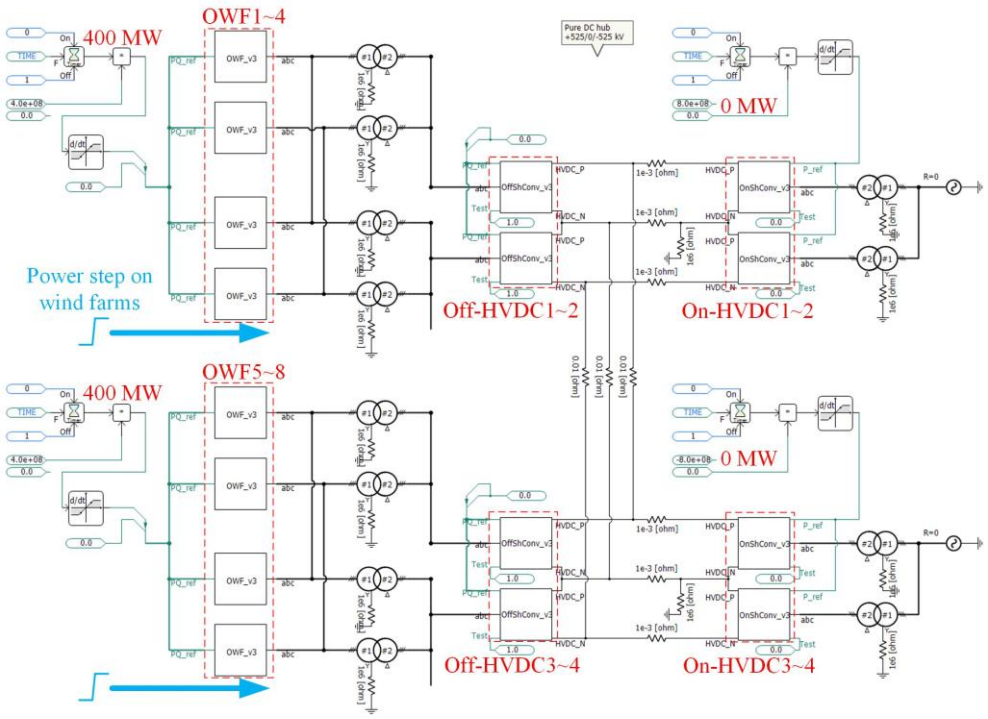

Figure 4.32: DC hub PSCAD model operating in power step on wind farm scenarios.

Figure 4.32 presents the developed DC hub PSCAD model operating in the scenarios of a power step on the wind farm. In fact, this case is similar to the study case 1, but the power has a step change on each wind farm in this case. The power generated by each wind farm is transferred to the onshore areas through the offshore and onshore HVDC converters.

The simulation results of the DC hub PSCAD model operating in the scenarios of a power step on the wind farm are presented in Figure 4.33. It can be seen that there is a 400 MW step change of the active power in each wind farm (such as OWF1). Thus, 800 MW of the active power is transferred to the offshore HVDC converters (such as Off-HVDC1 and Off-HVDC3). Then, the power in the DC hub is absorbed by the onshore HVDC converters (such as On-HVDC1 and On-HVDC3). Finally, the power is transferred to the onshore grids. It can be seen that each onshore and offshore HVDC converter has a power step response due to the power step of the wind farms. Besides, the DC voltage is equal to 525 kV plus the DC droop voltage.

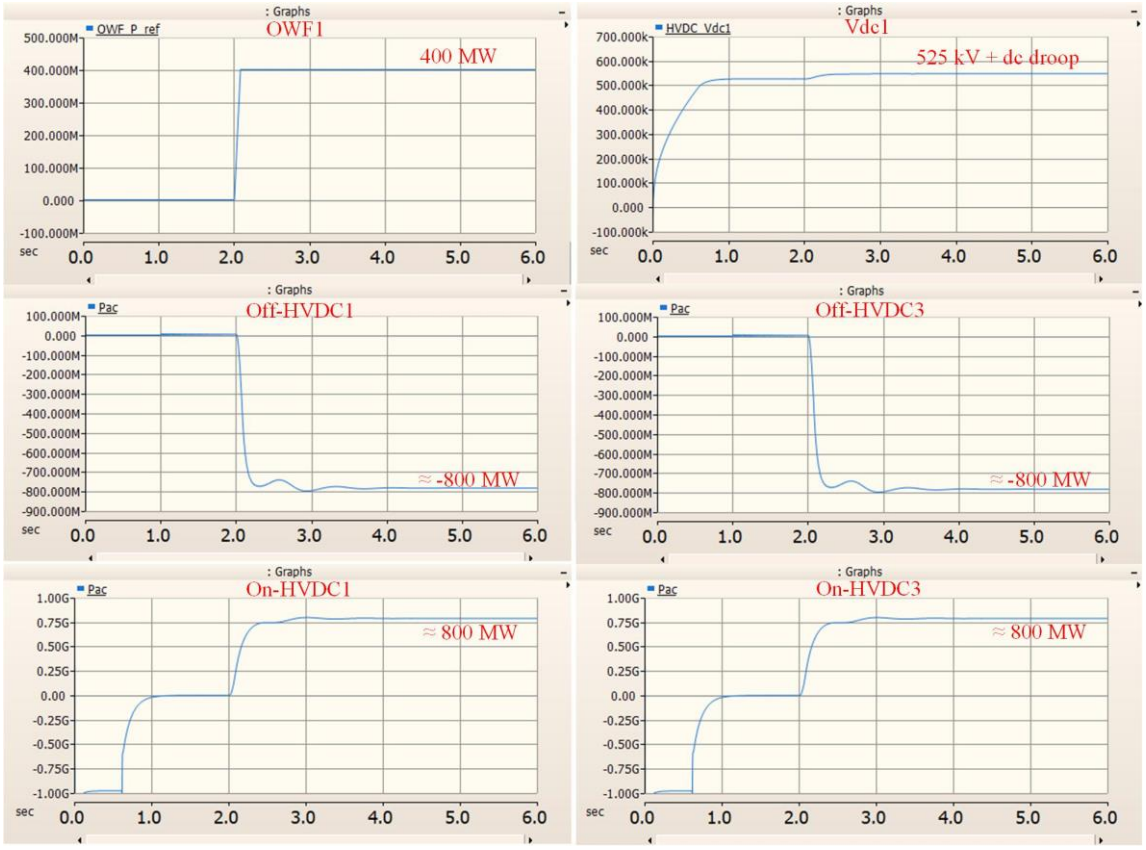

Figure 4.33: Simulation results of the DC hub PSCAD model operating in power step on wind farm scenarios.

Study Case 5A: Asymmetrical power from two wind farm areas

Figure 4.34 presents the developed DC hub PSCAD model operating in the asymmetrical power on wind farms scenario A, where only offshore wind farms 1, 2, 3, and 4 generate power, while the offshore wind farms 5, 6, 7, and 8 do not generate any power. In this case, the generated power from the offshore wind farms is transferred to offshore HVDC converters 1~2. Then, the power is further transferred to onshore HVDC converters 1~4 through the DC hub.

The simulation results of the DC hub PSCAD model operating in scenario A of the asymmetrical power on wind farms are presented in Figure 4.35. Each of the wind farms 1~4 generates 400 MW of active power. The power is only transferred to offshore HVDC converters 1~2, which is 800 MW for each offshore converter. When this power is injected to the DC hub, the DC voltage changes slightly around the nominal voltage 525 kV. Then, the power in the DC hub is absorbed by the onshore HVDC converters 1~4 equally. So, each onshore HVDC converter receives 400 MW of the active power. Finally, the power is transferred to the onshore grids.

Notably, since the simulation results of the onshore HVDC converters 2 and 4 are exactly the same as the simulation results of the onshore HVDC converters 1 and 3, they are not presented in Figure 4.35. Besides, the simulation results of the offshore HVDC converter 2 are exactly the same as the simulation results of the offshore HVDC converter 1. The simulation results of the OWF2, 3, and 4 are totally the same as the simulation results of the OWF1. So, they are not presented in Figure 4.35 either.

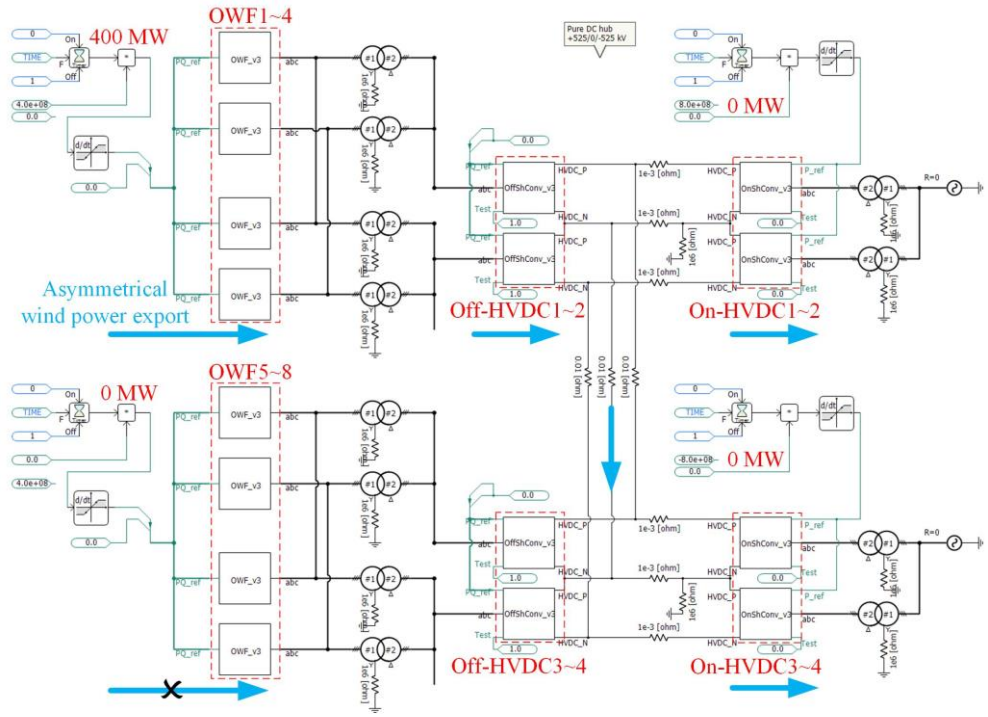

Figure 4.34: DC hub PSCAD model operating in asymmetrical power on wind farms scenario A.

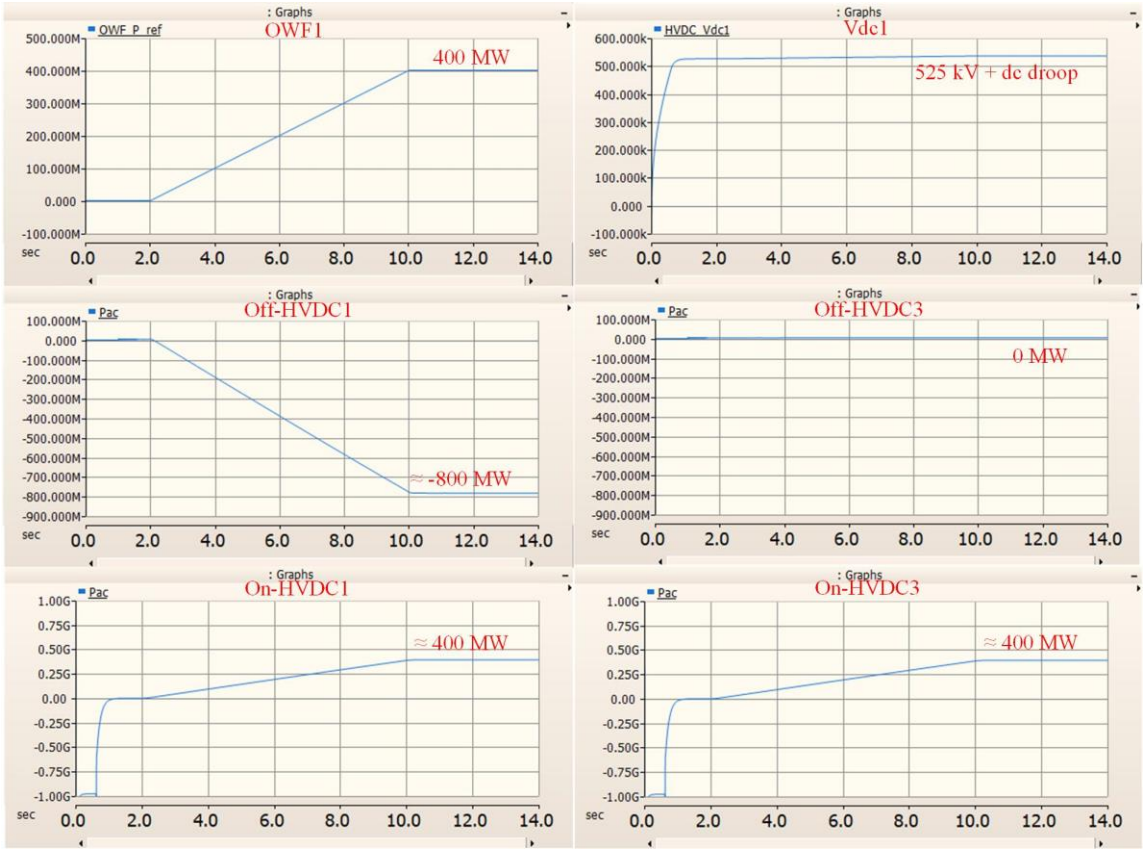

Figure 4.35: Simulation results of the DC hub PSCAD model operating in asymmetrical power on wind farms scenario A.

Study Case 5B: Asymmetrical power from one wind farm area

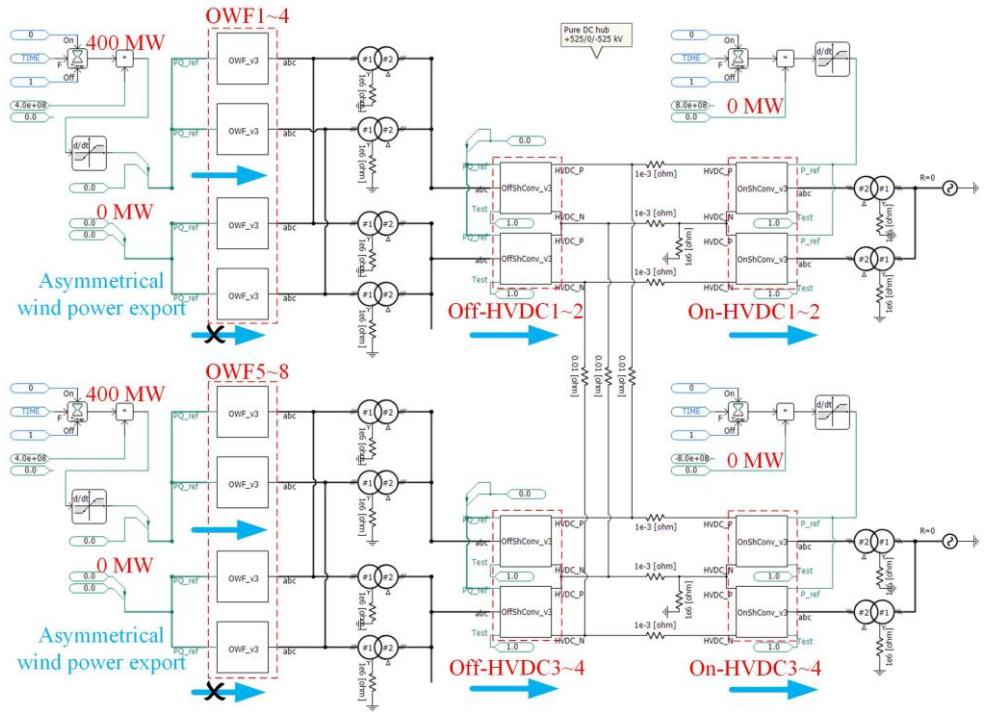

Figure 4.36: DC hub PSCAD model operating in asymmetrical power on wind farms scenario B.

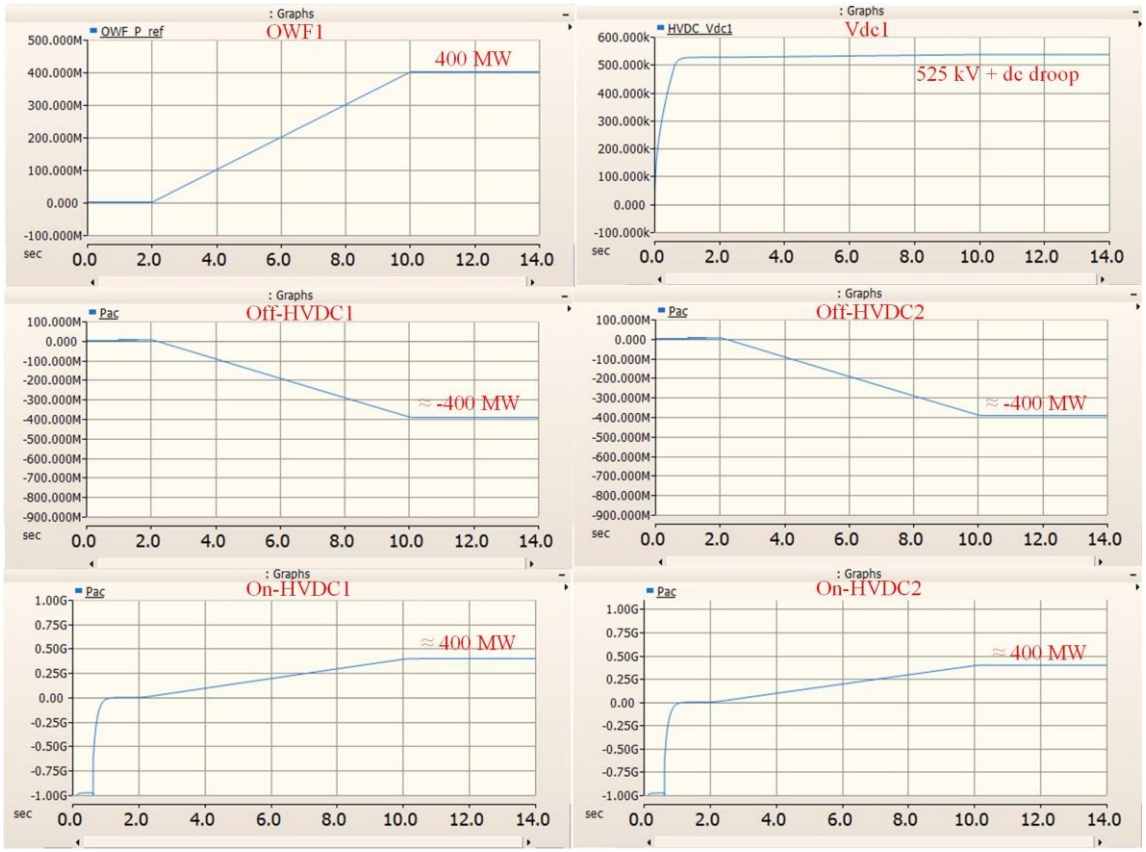

Figure 4.37: Simulation results of the DC hub PSCAD model operating in asymmetrical power on wind farms scenario B.

Figure 4.36 presents the developed DC hub PSCAD model operating in the asymmetrical power on wind farms scenario B, where only offshore wind farms 1, 2, 5, and 6 generate power, while the offshore wind farms 3, 4, 7, and 8 do not generate any power. In this case, each offshore HVDC converter receives 400 MW of the active power. Then, the power is further transferred to onshore HVDC converters 1~4 through the DC hub. So, each onshore HVDC converter receives 400 MW of the active power.

The simulation results of the DC hub PSCAD model operating in scenario B of the asymmetrical power on wind farms are presented in Figure 4.37. Each of the wind farms 1, 2, 5, and 6 generates 400 MW of active power. The power is transferred to offshore HVDC converters 1~4, and further to onshore HVDC converters 1~4. So, each offshore and onshore HVDC converter receives 400 MW of the active power. Finally, the power is transferred to the onshore grids.

Study Case 6: Asymmetrical power from bi-pole HVDC onshore converter

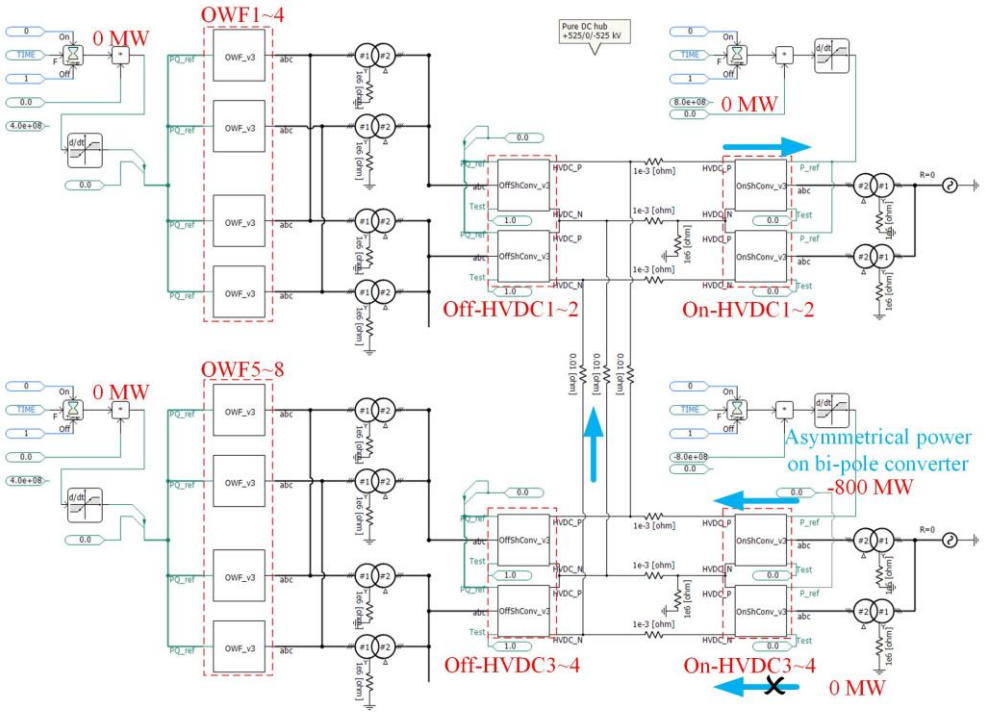

Figure 4.38: DC hub PSCAD model operating in asymmetrical power on bi-pole HVDC onshore converter scenarios.

Figure 4.38 presents the developed DC hub PSCAD model operating in the asymmetrical power on bi-pole HVDC onshore converter scenario, where only the onshore HVDC converter 3 injects power to the DC hub, while the onshore HVDC converter 4 does not inject any power. Then, the power is further transferred to onshore HVDC converters 1~2 through the DC hub.

The simulation results of the DC hub PSCAD model operating in the asymmetrical power on bi-pole HVDC onshore converter scenario are presented in Figure 4.39. It can be seen that the offshore wind farms do not generate any power in this case. So, the offshore HVDC converters receive zero power. Moreover, 400 MW of the active power only goes from the onshore HVDC converter 3 to the onshore HVDC converter 1. Since the onshore HVDC converter 4 does not inject any power to the DC hub, the onshore HVDC converter 2 receives zero power.

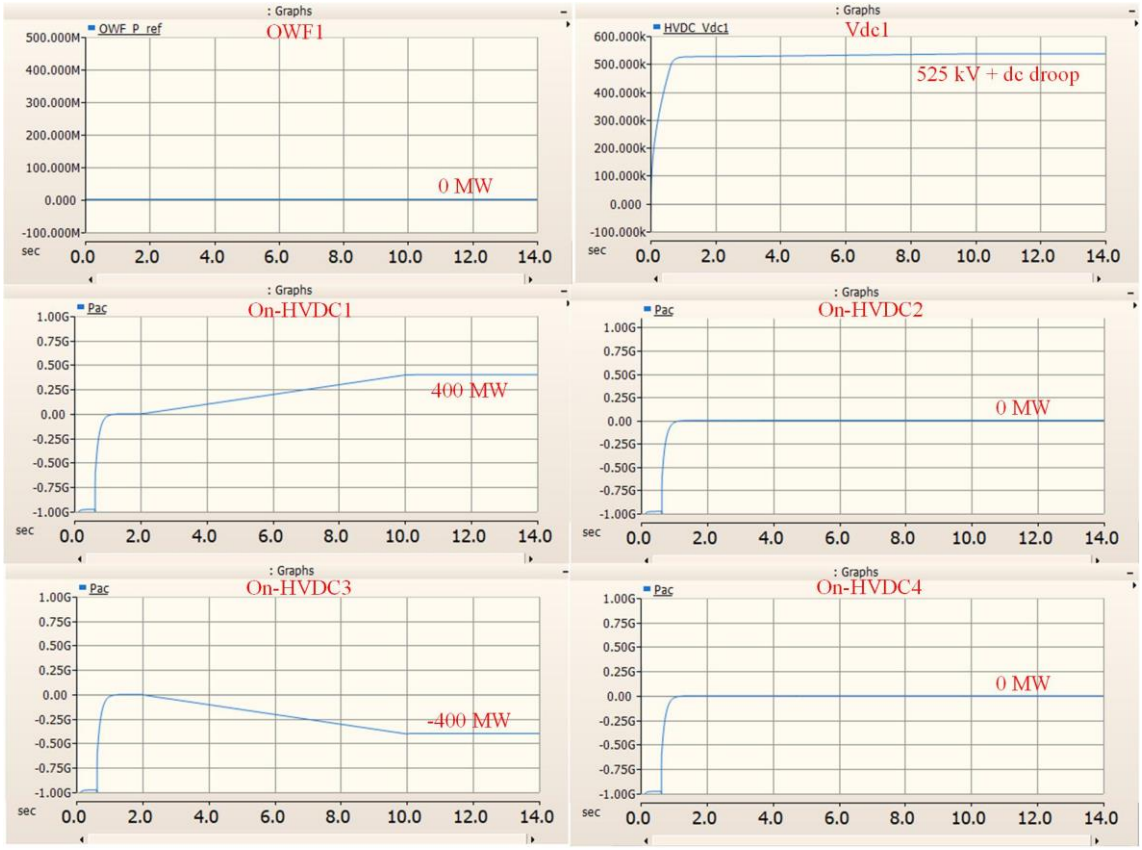

Figure 4.39: Simulation results of the DC hub PSCAD model operating in asymmetrical power on bi-pole HVDC onshore converter scenarios.

Study Case 7: Parameter sensitivity test

Figure 4.40 presents the developed DC hub PSCAD model operating in the parameter sensitivity test scenarios, where the DC droop coefficient of the onshore HVDC converter 3~4 is equal to 1.5 times the DC droop coefficient of the onshore HVDC converter 1~2. In this case, each offshore wind farm generates 400 MW of active power, and the power is transferred to the offshore HVDC converters and further to the onshore HVDC converters.

The simulation results of the DC hub PSCAD model operating in the parameter sensitivity test scenarios are presented in Figure 4.41. Each of the wind farms 1~8 generates 400 MW of active power (Figure 4.41 only shows the simulation results of the wind farm 1). The generated power is transferred to offshore HVDC converters 1~4, which is 800 MW for each offshore converter (Figure 4.41 only shows the simulation results of offshore HVDC converters 1 and 3). When this power is injected to the DC hub, the DC voltage changes slightly around the nominal voltage 525 kV. Then, the power in the DC hub is absorbed by the onshore HVDC converters 1~4 based on the DC droop coefficients. Since DC droop coefficient of the onshore HVDC converter 3~4 is equal to 1.5 times the DC droop coefficient of the onshore HVDC converter 1~2, the power of the onshore HVDC converters 1 and 3 are 960 MW and 640 MW (Notably, the ratio of the power is 1.5, same as the ratio of the DC droop coefficients). Finally, the power is transferred to the onshore grids.

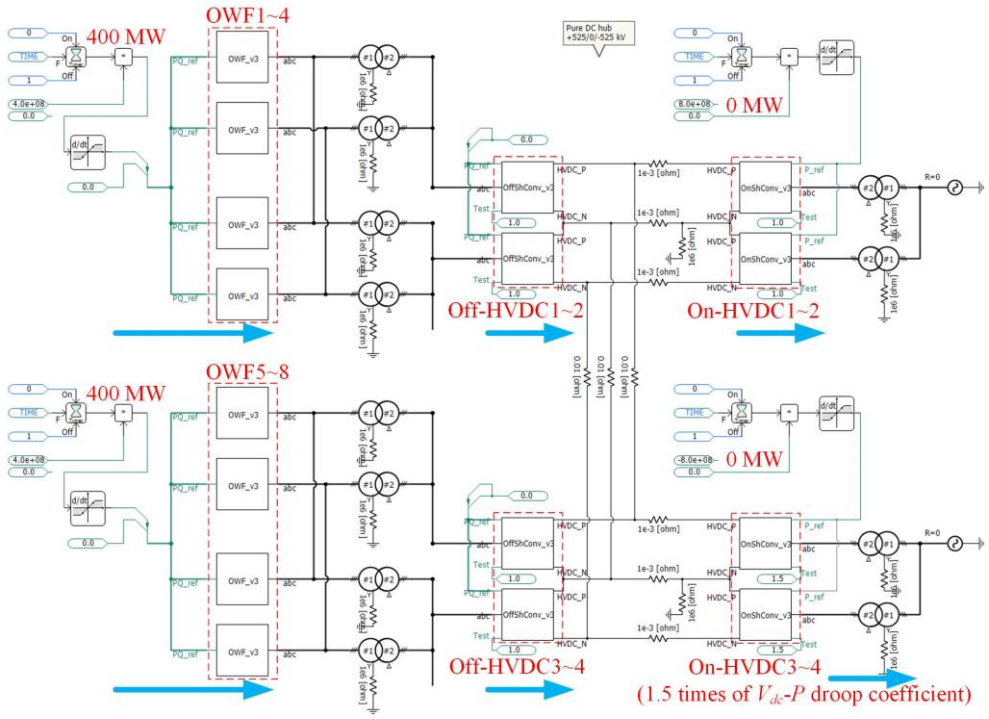

Figure 4.40: DC hub PSCAD model operating in parameter sensitivity test scenarios.

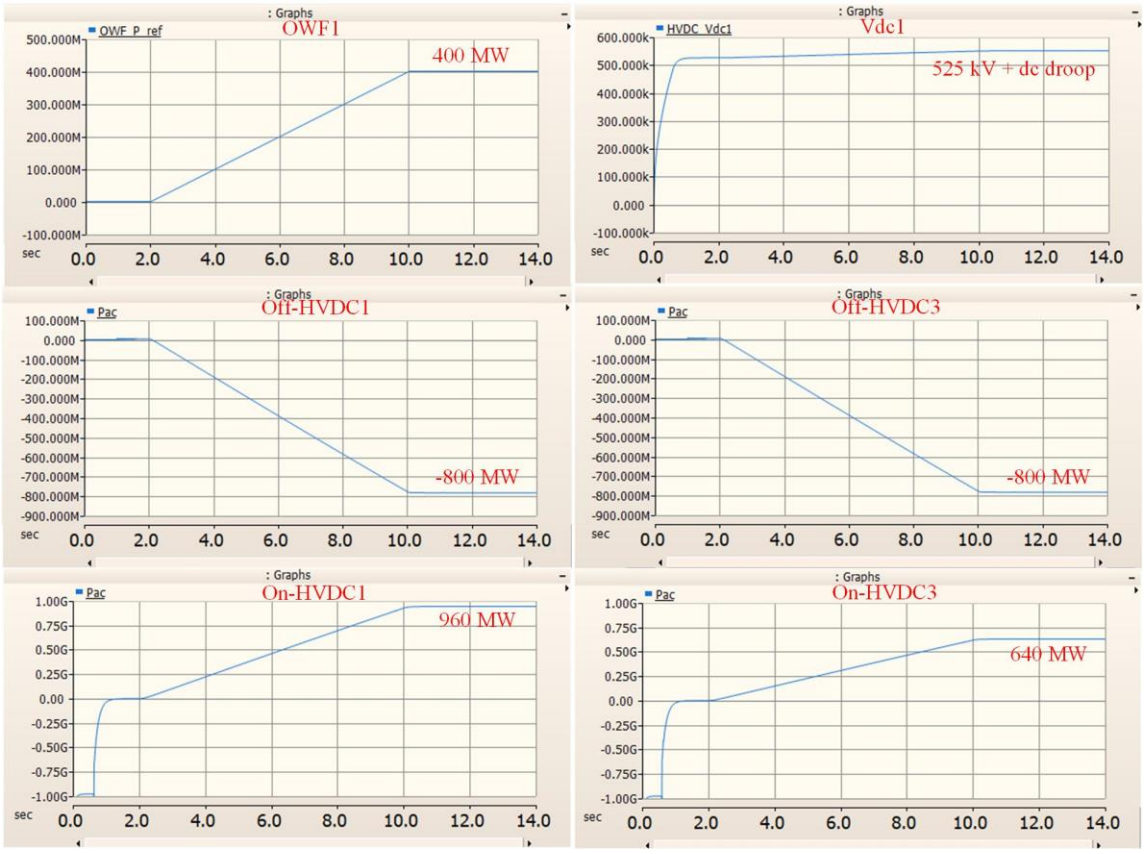

Figure 4.41: Simulation results of the DC hub PSCAD model operating in parameter sensitivity test scenarios.

Overall, the developed AC and DC hub PSCAD models have been tested in different scenarios under normal conditions. The simulation results illustrate that the selected GFM control scheme for the offshore HVDC converter and the DC droop control scheme for the onshore HVDC converter can operate stably in different scenarios.

4.5. HYBRID HUB MODEL DEVELOPMENT

Following the AC and DC hub model development, the hybrid AC and DC hub model is developed further. Based on the AC hub model development, it is found that the P reference should be given to the offshore HVDC converter to achieve the inter-area power transformation function. Differently, from the DC hub model development, it is found that the P reference should be given to the onshore HVDC converter to achieve the inter-area power transformation function. To avoid using different control solutions, a unified control solution that P reference is given to both onshore and offshore HVDC converters is proposed, which is presented in Figure 4.42.

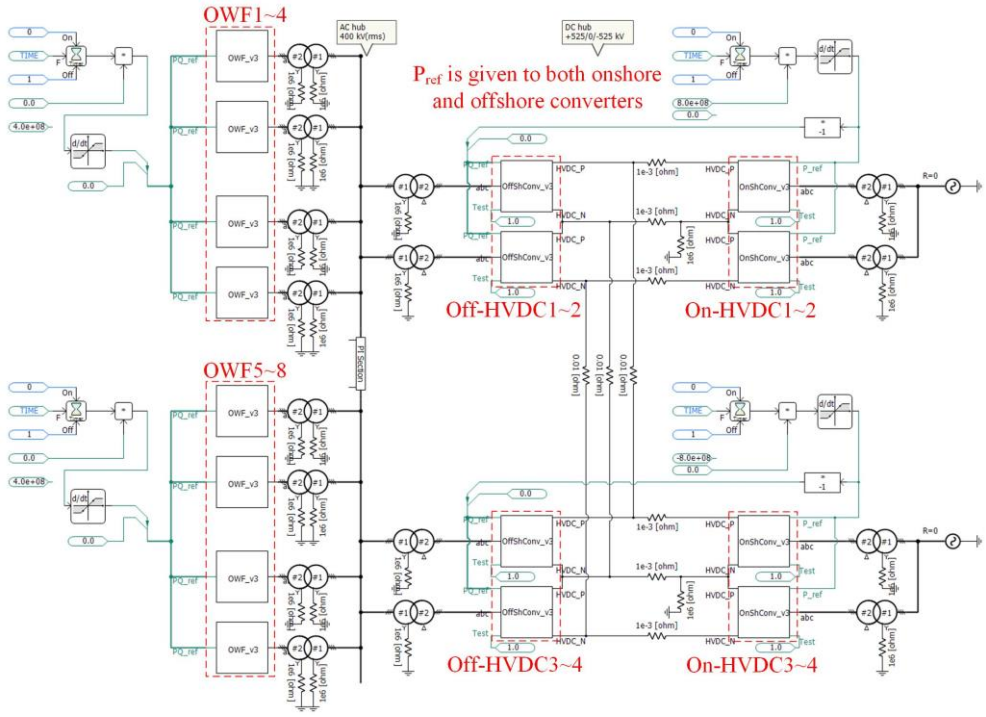

Figure 4.42: Hybrid hub PSCAD model with proposed unified control solution.

As shown in Figure 4.42, a unified control solution that P reference is given to both onshore and offshore HVDC converters is proposed. An important advantage of the proposed solution is that it is suitable for the AC hub, DC hub, and hybrid hub. Notably, the hybrid hub is equivalent to the AC hub when the DC interconnectors are disconnected, while the hybrid hub is equivalent to the DC hub when the AC interconnectors are disconnected. So, the simulation results of the hybrid hub model in different steady-state test cases are similar to the simulation results of either the AC hub or the DC hub. To avoid duplication, the simulation results of the hybrid hub are not presented.

In the next stage, the research focus will move to the AC and DC hub operating under abnormal conditions such as offshore AC grid voltage line-to-ground faults and trip of the offshore HVDC converter. In this case, additional control schemes for offshore and onshore HVDC converters need to be developed.

5. POWER FACTORY MODEL

Besides the PSCAD model, an equivalent Power Factory model was built. Both to confirm the primary results obtained with the initial PSCAD model and to allow for easier model exchange. Besides, Power Factory allows running RMS simulations, enabling much faster simulations for other types of studies.

Similar to the PSCAD model, 2 bipoles connect 8x500MW wind farms with HVDC connections. Voltage and power ratings, parameter tunings, etc are consistent with the original PSCAD model.

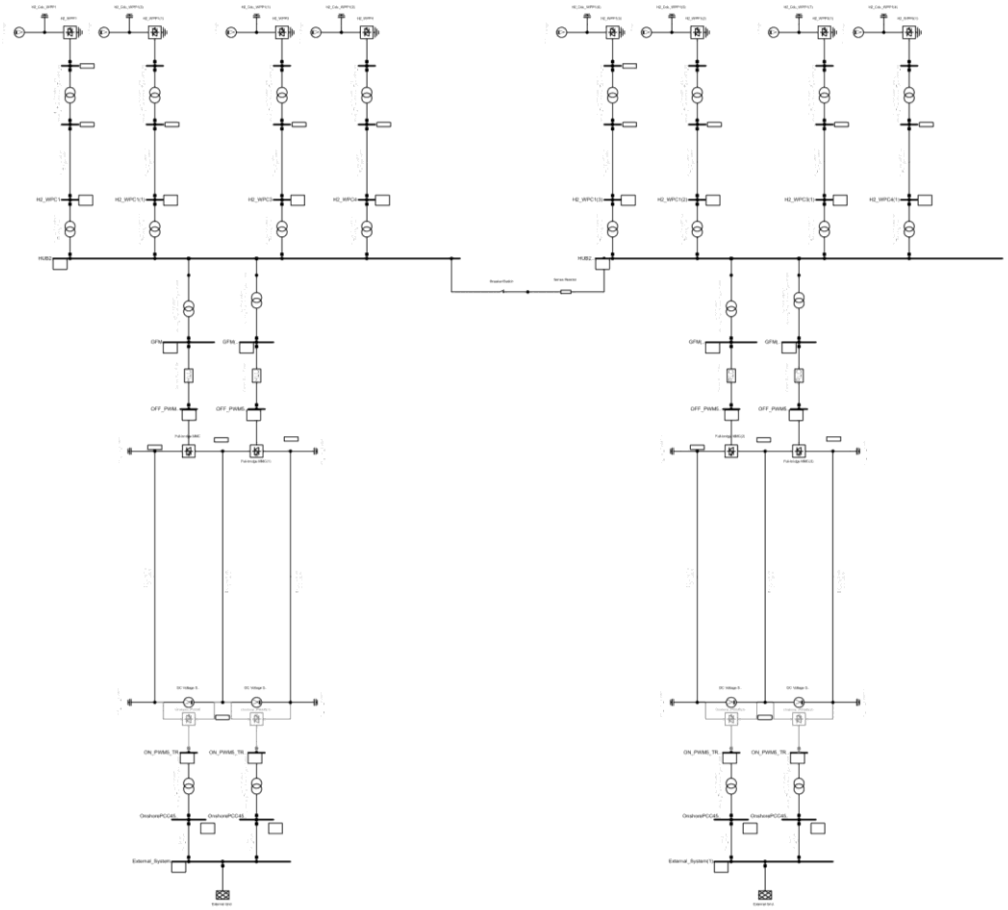

Figure 5.1: Power Factory model of the AC topology for the offshore energy hub

Regarding the controls, the model was designed in pu values and has the same control connections as the PSCAD. Both models use an outer loop to synchronize with the grid through power balancing. The voltage is set through single or double inner loops, for the single or multiple loop control respectively.

Figure 5.2 below depicts the control schematic for the single loop control. Most of the control is in the “Grid forming control” block, including the power synchronisation as well as the PI loop over the voltage. The “Output voltage calculation” sums up the reference voltage and the virtual impedance contribution and performs the inverse Park transform on the voltages. Finally, “p_set”, “q_set” and

"u_set" are the reference values, set during the initialisation. They are therefore based on the power flow results.

Figure 5.2: Power Factory single loop control model

The voltage measurement is in the alpha-beta components. This makes a difference in the simulation strategy, as the model can therefore be run in RMS.

On the other hand, the multiple loop control model is shown in Figure 5.3 below. The "PSC" block corresponds to the power synchronisation control, including the V-Q and Phi-P droops. The output angle "omega" is used as a reference for the converter. Following, the voltage loop control uses a PI to ensure that the d and q voltages follow the references provided by the "Virtual Impedance" block. The "Current Control" is the cascaded control, acting faster than the previous ones. The latest is particularly useful during fault events when the current is to be limited. Finally, the "PLL" and "Angle" blocks were used for debugging purposes and visualisation purposes, allowing to depict the grid voltage angle in time.

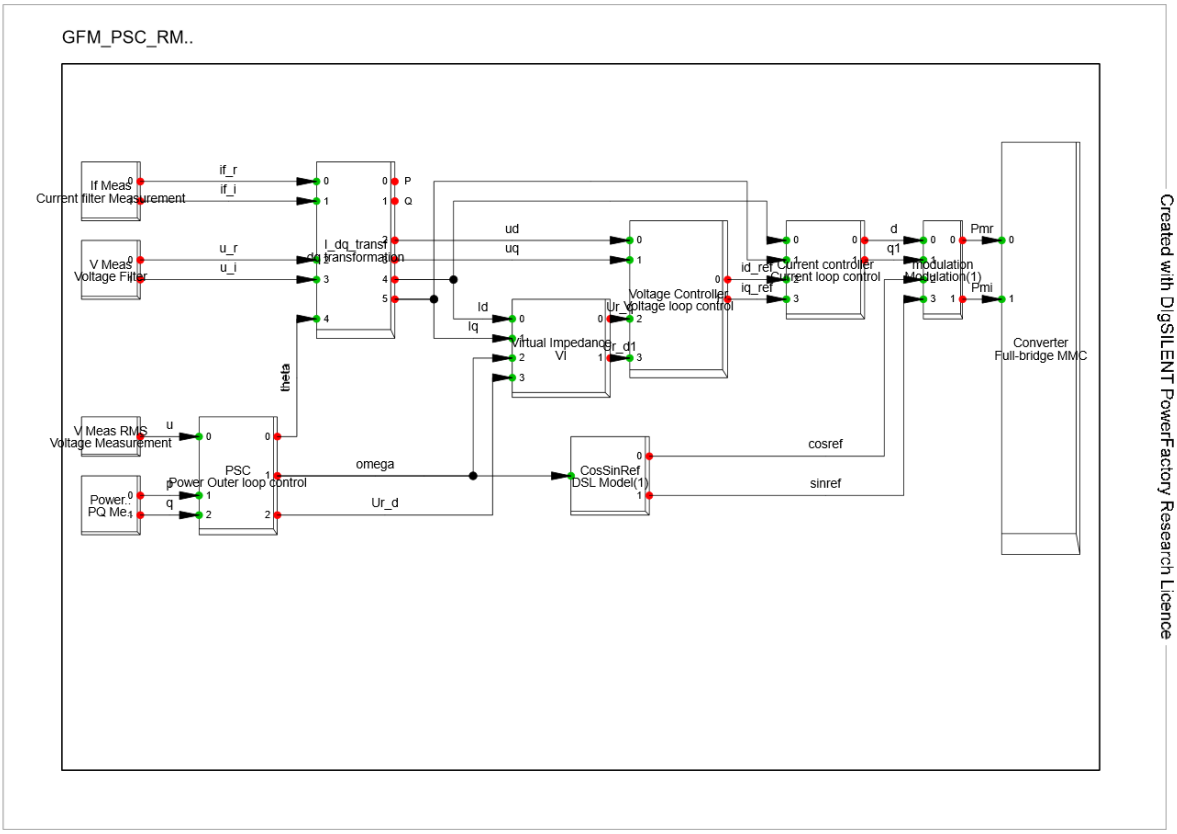

Figure 5.1: Power Factory multiple loop control model

To confirm the models, time simulations have been carried out, allowing us to compare the performances.

6. MODEL COMPARISON

Both models have been compared during a power step from the wind farms. As presented in the previous sections, the wind farm power ramp is limited to 0.1pu/sec. No large transient performances are therefore compared here. The main point is to compare the steady-state operation and ensure similar parameters.

Comparison is achieved by plotting the active and reactive power, the voltage and the frequency. Figure 6.1 presents the results for the single loop control, whereas Figure 6.2 plots the 4 values for the multiple loop control strategy.

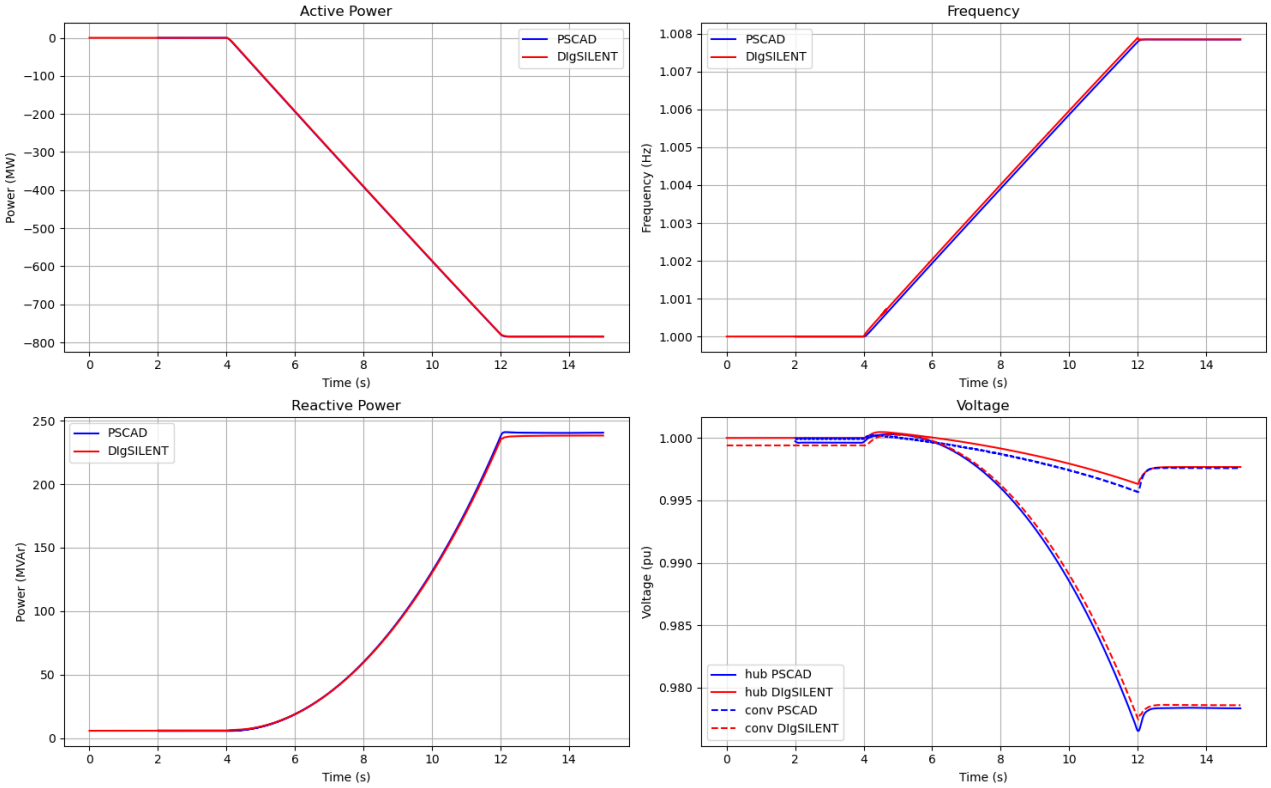

Figure 6.1: Load step 0-400MW for the single loop control

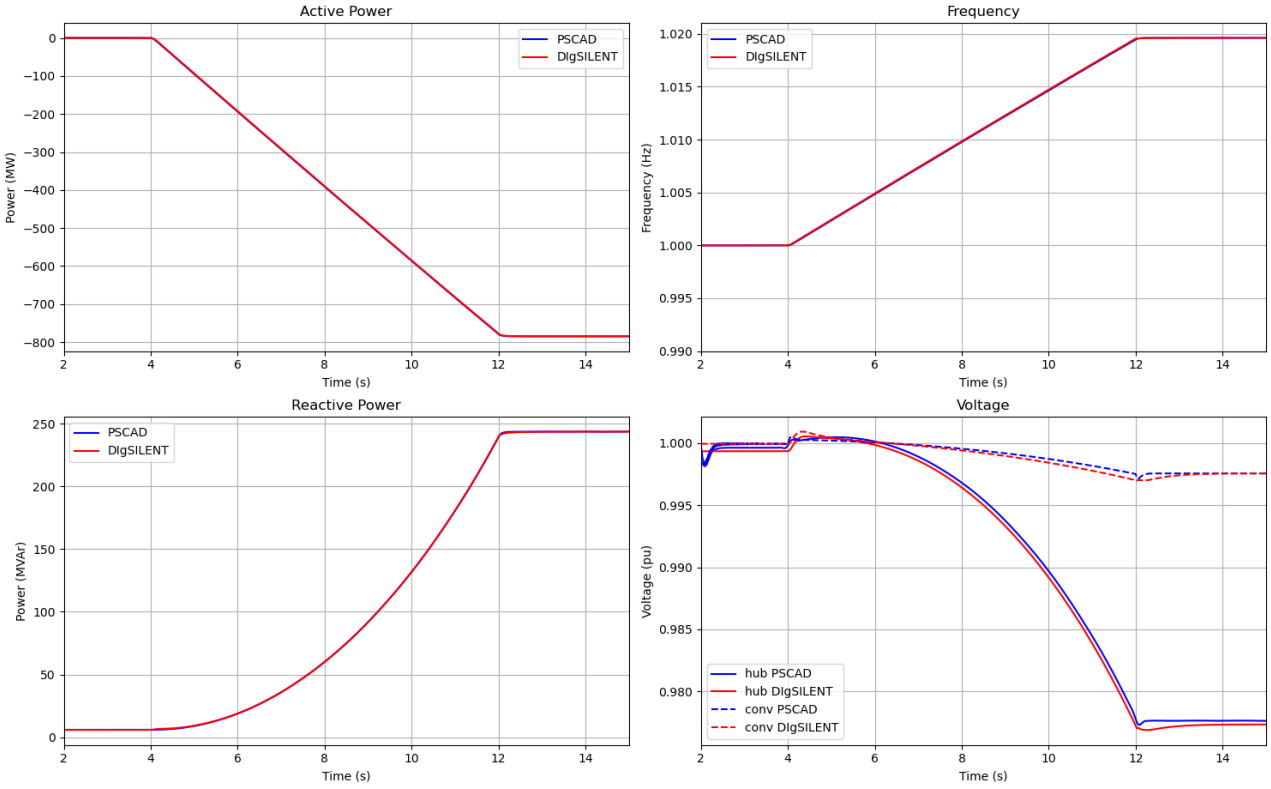

Figure 6.2: Load step 0-400MW for the multiple loop control

Table 6.1 below presents the relative errors at t=15s, i.e. after the step of power. It considers the PSCAD model as reference values. Mismatches remain under 5% for all the variables.

Table 6.1: Relative difference between PSCAD and PF models

Rel. error [%]	Active Power	Reactive Power	Frequency	Hub Voltage	Conv. Voltage
Single loop	0.01	0.95	0.0003	1.97	1.90
Multiple loop	0.01	0.027	0.0007	0.029	0.0002

A second simulation highlights the transient behaviour of both models. By removing the power ramp in

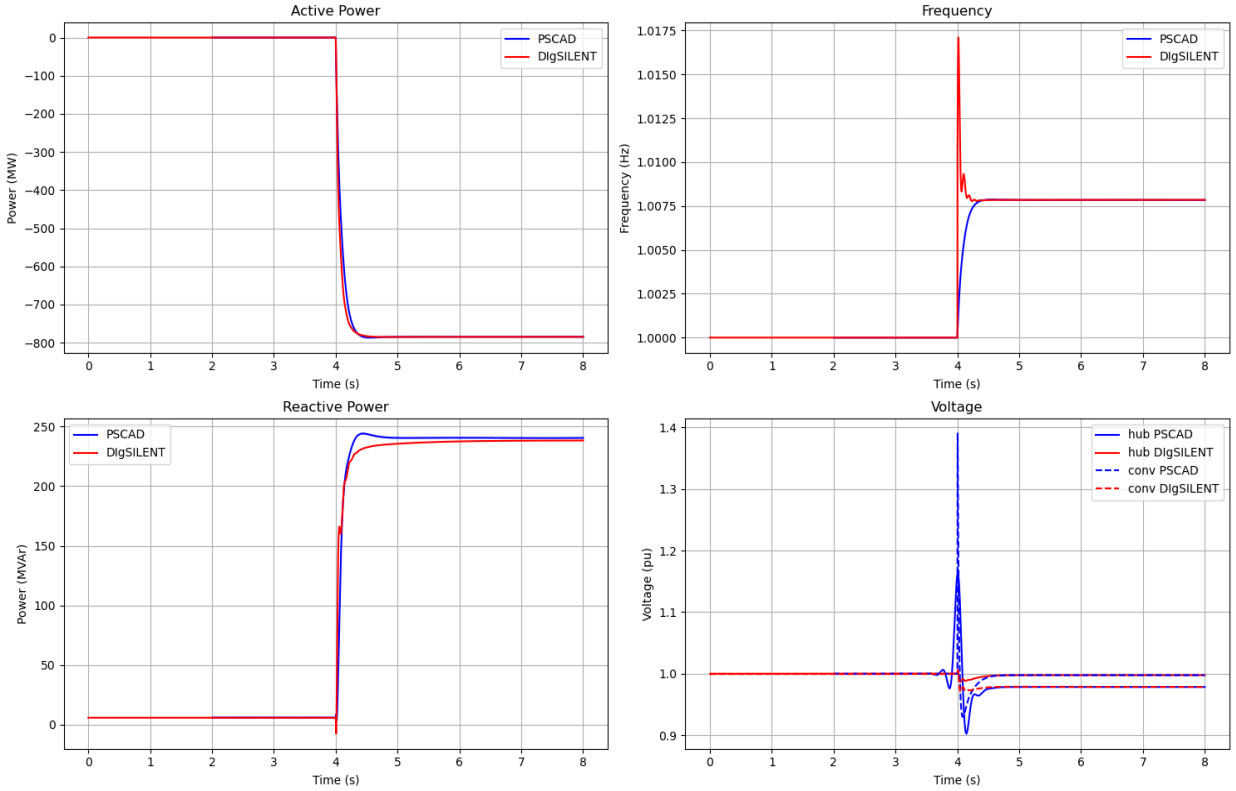

Figure 6.3: 0-400MW power jump, Single Loop control

the wind farm controller, a large but not realistic power step is run. Results are shown in Figure 6.3 and Figure 6.4. One can see that the steady-state difference has not changed compared to the limited ramp rate scenario, but some differences can be noticed in the transient behaviour.

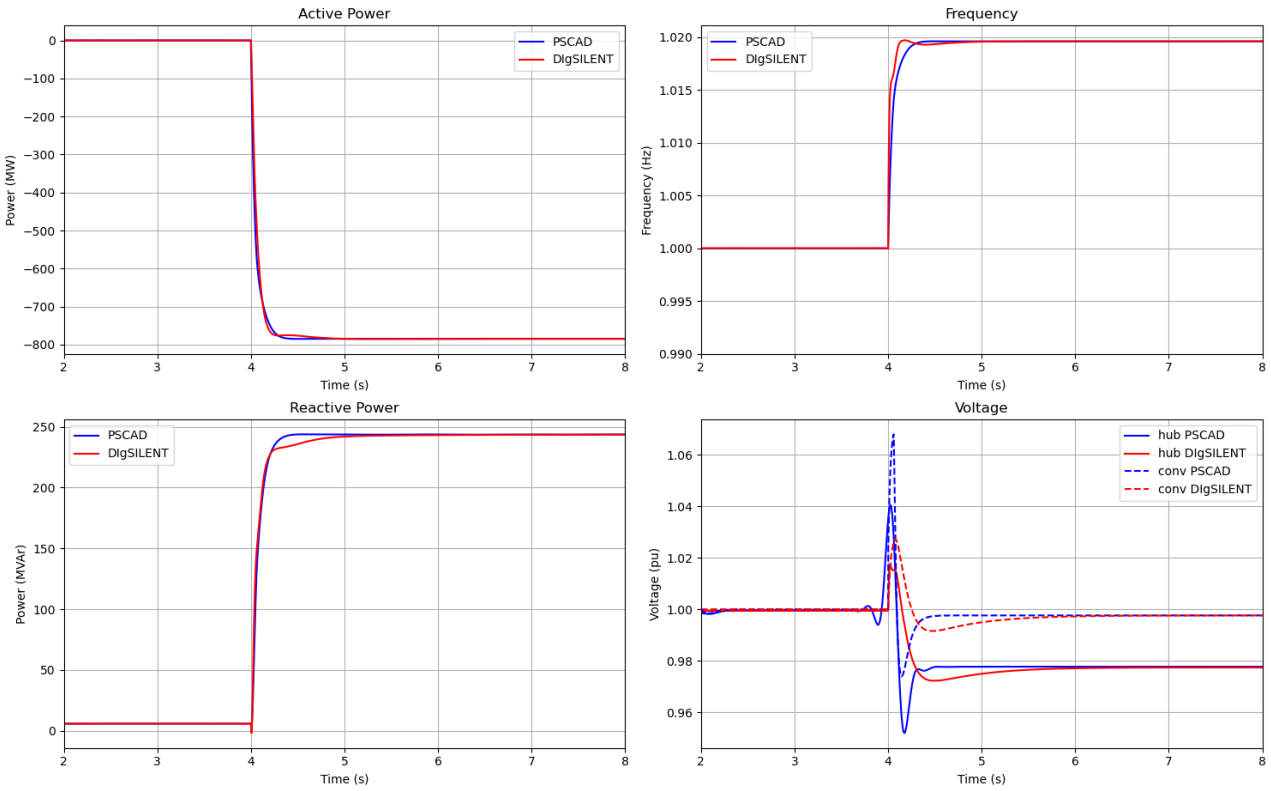

Figure 6.4: 0-400MW power jump, Multiple Loop control

Time simulations have confirmed the good match between the models built in two separate simulation software. The normal operation scenario presents very close results. However, the power factory models allow for much faster simulation (approximately 10 times faster). Power Factory will be, therefore, preferred for long-term simulations such as hub planning and power flows, whereas the PSCAD model will investigate the transient behaviours and fault management with potential energy dissipation.

7. CONCLUSIONS

Overall, the AC hub models have been developed in both PSCAD and Power Factory simulation platforms. The developed AC hub PSCAD and Power Factory models with both the single-loop GFM control scheme and the multiple-loop GFM control scheme work well in the selected test cases. Besides, simulations have confirmed a good match between the PSCAD models and Power Factory models. Moreover, the DC hub model has been developed in PSCAD simulation platform. Simulation results indicate that the developed DC hub PSCAD model with DC droop control works well in the selected test cases.

In the next stage of WP2, the AC and DC hubs operating in abnormal conditions such as offshore AC grid voltage line-to-ground faults and trip of the offshore HVDC converter will be evaluated, where the detailed switching model of the MMC is planned to be used. Additional control schemes for GFM

converters, such as the LVRT scheme and energy dissipation scheme, need to be considered to stabilise the offshore energy hub in different fault scenarios.

8. REFERENCES

[1] EUDP, “Offshore Energy Hubs”, [Online]. Available: https://offshoreenergyhubs.eu/.

[2] “Offshore Energy Hubs - Feasibility assessment of hub topologies”, Offshore Energy Hubs Project, Technical Report, 2024.

[3] A. Antonio-Ferreira, C. Carlos-Rodriguez, and O. Gomis-Bellmunt, “Modulation techniques applied to medium voltage modular multilevel converters for renewable energy integration: A review”, Electric Power Systems Research, vol. 155, pp. 21-39, 2018.

[4] “Guide for the Development of Models for HVDC Converters in a HVDC Grid”, CIGRE, Technical Brochures, Reference 604, 2014.

[5] S. D’Arco and J. A. Suul, “Virtual synchronous machines - classification of implementations and analysis of equivalence to droop controllers for microgrids,” in Proc. IEEE Grenoble Conf., 2013, pp. 1–7.

[6] Q. Zhong, P. Nguyen, Z. Ma, and W. Sheng, “Self-synchronized synchronverters: Inverters without a dedicated synchronization unit,” IEEE Trans. Power Electron., vol. 29, no. 2, pp. 617–630, Feb. 2014.

[7] H. Bevrani, T. Ise, and Y. Miura, “Virtual synchronous generators: A survey and new perspectives,” Elect. Power Energy Syst, vol. 54, pp. 224–254, 2014.

[8] L. Zhang, L. Harnefors, and H. Nee, “Power-synchronization control of grid-connected voltage-source converters,” IEEE Trans. Power Syst., vol. 25, no. 2, pp. 809–820, May 2010.

[9] W. Zhang, A. M. Cantarellas, J. Rocabert, A. Luna, and P. Rodriguez, “Synchronous power controller with flexible droop characteristics for renewable power generation systems,” IEEE Trans. Sustain. Energy, vol. 7, no. 4, pp. 1572–1582, Oct. 2016.

[10] M. Lu, “Virtual Oscillator Grid-Forming Inverters: State of the Art, Modeling, and Stability,” IEEE Trans. Power Electron., vol. 37, no. 10, pp. 11579-11591, Oct. 2022.

[11] L. Huang, C. Wu, D. Zhou and F. Blaabjerg, “Impact of Virtual Admittance on Small-Signal Stability of Grid-Forming Inverters,” 2021 6th IEEE Workshop on the Electronic Grid (eGRID), New Orleans, LA, USA, 2021, pp. 1-8.

[12] T. M. Haileselassie and K. Uhlen, “Impact of DC Line Voltage Drops on Power Flow of MTDC Using Droop Control,” IEEE Trans. Power Syst., vol. 27, no. 3, pp. 1441-1449, Aug. 2012.

[13] “Functional requirements for HVDC grid systems and subsystems”, InterOPERA Project, Technical Report, 2024.

[14] X. Lu, J. M. Guerrero, K. Sun and J. C. Vasquez, “An Improved Droop Control Method for DC Microgrids Based on Low Bandwidth Communication With DC Bus Voltage Restoration and Enhanced Current Sharing Accuracy,” IEEE Trans. Power Electron., vol. 29, no. 4, pp. 1800-1812, April 2014.